**People's Democratic Republic of Algeria**

**وزارة التعليم العالي والبحث العلمي**

**Ministry of Higher Education and Scientific Research**

**Mohamed El Bachir Elibrahimi**
**University – Bordj Bou Arréridj**

**Faculty of Science and Technology**

**Department of Materials Sciences**

**جامعة محمد البشير الإبراهيمي « برج بوعريريج »**

**كلية العلوم والتكنولوجيا**

**قسم علوم المادة**

# *Dissertation submitted for obtaining academic Master's degree*

## *Sector: Physics*

## *Option: Physics of Materials*

## ***Title***

# *Synthesis, structure and properties of $Re_2 (Ti_{0.5},Zr_{0.5}) O_7$ pyrochlore*

**Presented by: Chebli Samira**

**Defended on 28/06/2025, before the jury composed of:**

| **Name & First name** | **Grade** | **Establishment** | **Quality** |
|---|---|---|---|
| **Dr. BENCHIHEUB Nadjat** | MCA | Univ. of BBA | President |
| **Dr. REDAOUI Djaida** | MCB | Univ. of USTHB | Supervisor |
| **Dr. BENDJEFFAL Abdelhak** | MCB | Univ. of BBA | Examiner |
| **Dr. MIHOUBI Karima** | MCB | Univ. of BBA | Examiner |

**Academic Year: 2024/2025**

# Dedication

بسم الله الرحمن الرحيم

In the name of Allah, the Most Gracious, the Most Merciful

This work is dedicated to:

My husband and my children.

My teachers.

And to myself.

And everyone who left their mark on this journey.

# *Gratitude*

*With the utmost appreciation and gratitude, I extend my sincere thanks and profound appreciation to my supervisor, Professor Dr.* ***REDAOUI Djaida****, who was the motivation and inspiration for my efforts. By accepting to supervise this Dissertation, and with her wise guidance, precise advice, valuable observations, and continuous dedication to this work, which she considered part of her own effort, she spared no effort to ensure its completion under the best circumstances. All of this was done with a welcoming smile and broadmindedness. May Allah reward her abundantly on my behalf, and may Allah bless her time and work, with my sincere wishes for her continued excellence and success to reach the highest ranks in her academic career.*

*I also extend my deep thanks and immense gratitude to the professors of the Faculty of Science and Technology, Department of Materials Science, at Bachir El Ibrahimi University in Bordj Bou Arréridj, and I specifically mention Professor* **KOUSSA W.** *for his exerted efforts.*

*I am honored and grateful that Dr.* ***BENCHIHEUB Nadjat*** *has accepted to chair the jury. My sincere gratitude goes to Dr.* ***BENDJEFFAL Abdelhak*** *and to Dr.* ***MIHOUBI Karima*** *for accepting to participate as an examiner on this jury.*

*Finally, I would like to express my deepest thanks to all the members of the Physics and Chemistry of Materials Lab at the University of Msila and the University of bejaia.*

*And to everyone who embraced me with open arms, followed my progress sincerely, and eased my path in preparing this dissertation, which we hope will be a valuable reference.*

# Contant

## *Chapter One: Bibliographic Study*

## *Chapter Two: Materials & Methods*

### *Chapter Three: Results & Discussion*

# General Introduction

# General Introduction

Throughout history, material development has relied on multiple approaches. Scientists often question the limited effectiveness of traditional design concepts, pushing them to explore new possibilities in pursuit of unfamiliar discoveries and to achieve qualitative leaps. Among these approaches, chemical composition modification—known as alloying in metallic systems and doping/hybridization in non-metallic systems—is the most common method for designing new materials. Despite the success of traditional alloy design strategies in producing useful and valuable materials, they are inherently limited; they do not allow for the exploration of the full potential compositional space of alloys. To overcome these limitations, a design strategy emerged that relies on combining several principal elements in similar proportions, known as Multi-Principal Element Alloys. In these alloys, the single solvent element is replaced by an equal or near-equal mixture of two or more elements, enabling the exploration of new regions in the compositional space of alloys. This design creates unique atomic environments that result in unpredictable properties due to the complex interactions between components. This promising category forms advanced materials that exhibit outstanding performance in advanced engineering applications.

For many centuries, the concept of alloy design remained based on the same model, until the beginning of the current millennium when a new class emerged, known as High-Entropy Alloys (HEAs). Researcher Yeh et al. first defined them as modern materials consisting of a homogeneous mixture of five or more principal chemical elements, distributed in equal or near-equal atomic proportions. The high configurational entropy contributes to reducing the system's Gibbs free energy, which enhances the stability of the solid phase of these alloys. Compared to traditional alloys, unique phenomena emerge in High-Entropy Alloys such as: severe lattice distortion, sluggish diffusion, and the significant cocktail effect. These mechanisms collectively led to the discovery of unprecedented crystalline compositions and alloys with exceptional mechanical and physical properties, surpassing their traditional counterparts. These advantages have stimulated the development of the field to include a broader category known as High-Entropy Materials (HEMs), which includes non-metallic systems.

Since 2004, research efforts have been made to explore non-metallic high-entropy materials such as nitrides and carbides. However, interest in High-Entropy Oxides (HEOs) saw a qualitative leap after the publication of the pioneering research by Rost et al. in 2015, which demonstrated—for the first time—the possibility of incorporating five metal elements (Co, Cu, Mg, Ni, Zn) into the cation sublattice sites of the rock-salt structure, forming the homogeneous compound $(Co_{0.2}Cu_{0.2}Mg_{0.2}Ni_{0.2}Zn_{0.2})O$. This compound was characterized by the presence of a single stable crystalline phase, challenging previous expectations that ruled out the possibility of forming multi-cation oxides of such complexity (five or more cations in equiatomic ratios). This achievement represents a conceptual shift in materials science, due to the absence of experimental evidence or theoretical models supporting this possibility prior to the mentioned study.

In this context, the current study focuses on high-entropy oxides with a pyrochlore structure, which exhibit unique properties such as high thermal stability and enhanced ionic conductivity, making them promising candidates for applications in thermal barrier coatings (TBCs) and solid-state electrolytes.

**Chapter I:** Provides a comprehensive literature review of the classification of high-entropy oxides and their physicochemical properties, with a focus on applying Pauling's Rules to cation selection.

**Chapter II:** Details the experimental methods used to prepare samples, including ball milling and sintering techniques, alongside characterization tools such as X-ray diffraction (XRD) and scanning electron microscopy (SEM).

**Chapter III:** Discusses results analysis, including:

- Confirmation of pyrochlore phase stability via ionic radius ratio calculations.
- Study of thermal behavior and coefficient of thermal expansion (CTE) using thermogravimetric analysis (TGA/DTA) and dilatometry.

- Microstructural analysis and elemental distribution via energy-dispersive X-ray spectroscopy (EDS).

The study concludes by emphasizing the importance of high-entropy oxides in high-temperature engineering applications, highlighting experimental contributions to understanding their stability mechanisms and functional performance.

# Chapter One

# Bibliographic Study

This chapter focuses on a bibliographic overview of the physicochemical properties, including the structure, preparation methods, and applications of ceramics and high-entropy oxide ceramics (HEOCs).

## I.1. Introduction

Ceramics represent one of humanity's oldest engineered materials, with archaeological evidence tracing ceramic production back to approximately 15,430 years ago in Yuchanyan Cave, Hunan Province, China, as confirmed by radiocarbon dating of associated charcoal and bone collagen [1]. This ancient craft has evolved into a sophisticated field of materials science that bridges traditional manufacturing with cutting-edge technology.

Materials are fundamentally categorized into metals, polymers, and ceramics based on their chemical bonding, forming the core of engineering and materials science. Among these, ceramics stand as the oldest manufactured material.

Figure I.1 illustrates the historical timeline of materials, highlighting ceramics' enduring significance from prehistoric times to modern applications. The term "ceramic" itself, derived from the Greek "keramos" meaning "burned stuff," aptly describes materials that acquire their characteristic properties through high-temperature processing [2].

Traditional ceramics are typically defined as non-metallic, inorganic, and predominantly polycrystalline, containing at least 30% crystalline compounds. Ceramic grains, usually ranging from 1 to 50 µm, are observable under a microscope [2,3]. Over centuries, ceramic processing techniques have evolved from simple clay firing to sophisticated methods including powder synthesis, shaping, drying, and sintering, as detailed in comprehensive reviews of ceramic processing and sintering technologies [3].

Today, the ceramic family encompasses a diverse range of materials beyond traditional pottery, including advanced ceramics for structural applications and specialized bioceramics for medical uses [4]. Modern ceramics exhibit a broad spectrum of thermal, optical, mechanical, electronic, and biological properties, and are composed of inorganic compounds such as silicates, simple and complex oxides, nitrides, and sometimes monoxides [2,4].

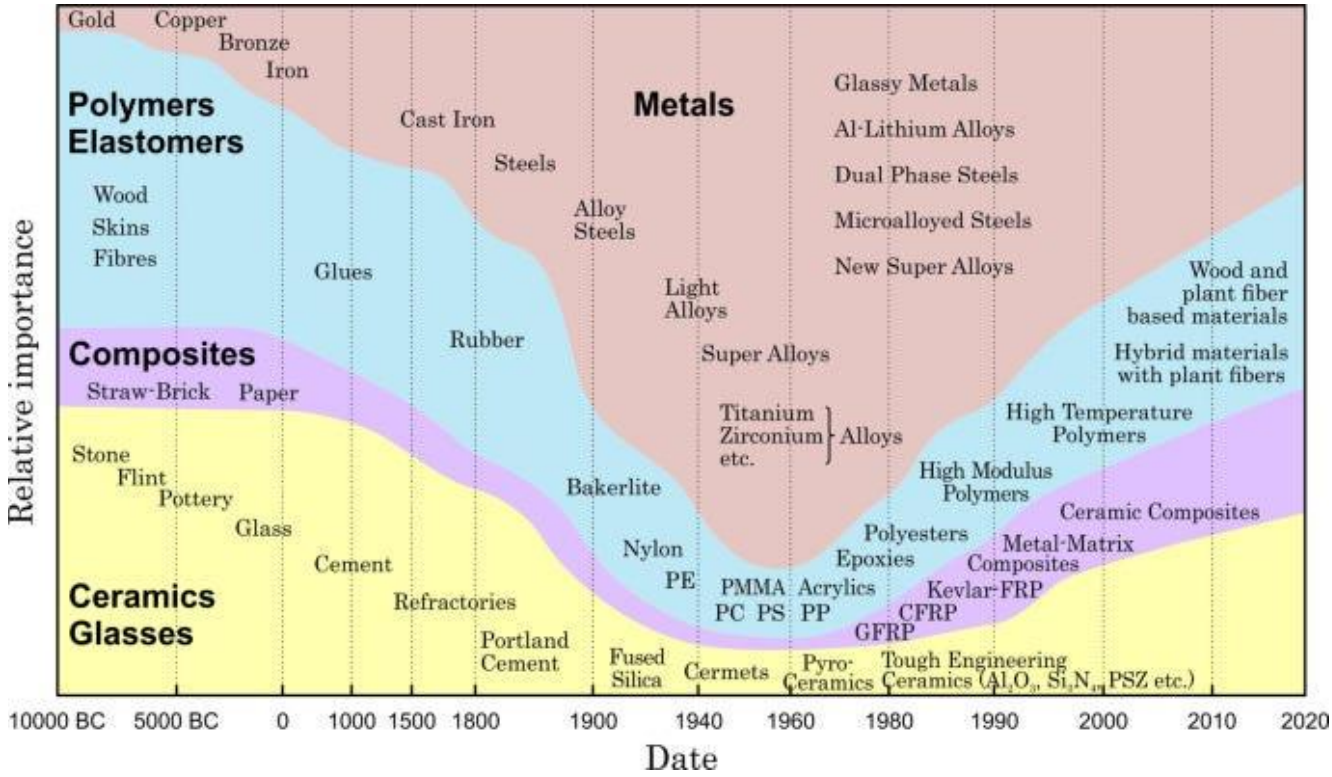

**Figure I.1**: Timeline of materials development [2].

## I.2. Types of Ceramics

Ceramics are broadly classified into two categories based on their composition, processing, and applications: traditional ceramics and advanced ceramics [2].

### I.2.1. Traditional Ceramics

Traditional ceramics, representing the earliest engineered materials, date back to approximately 15,430 years ago, as evidenced by ceramic remnants from Yuchanyan Cave, Hunan Province, China [1]. These materials are primarily derived from naturally occurring raw materials such as clays, micas, feldspars, and quartz, with some non-silicate minerals (e.g., magnesite) or simple oxides also used [2].

Common applications include general pottery, Chinese porcelain, sanitary ware, bricks, and tiles [2]. Their processing typically involves shaping and firing natural minerals at moderate temperatures, resulting in polycrystalline microstructures with silicate-based compositions [2,3].

### I.2.2. Advanced Ceramics

The limitations of traditional ceramics in meeting modern technological demands spurred the development of advanced ceramics, also termed functional and structural ceramics [2]. These materials are synthesized from high-purity, nanoscale or microscale precursors, including alumina ($Al_2O_3$), magnesia (MgO), silicon carbide (SiC), silicon nitride ($Si_3N_4$), and other simple or complex oxides [2,3]. Advanced ceramics are engineered for specialized applications across diverse fields, Electrical (Insulators, capacitors), Optical (Transparent ceramics, laser hosts), Medical (Bioceramics for implants (e.g., hydroxyapatite)) [4], Thermal (Refractory components, thermal barrier coatings) [5].

Unlike traditional ceramics, advanced ceramics prioritize tailored combinations of properties (e.g., high strength, wear resistance, biocompatibility) over individual characteristics, enabling their use in extreme environments [2,4].

## I.3. Transition from Traditional Ceramics to High-Entropy Ceramics

The evolution of ceramics from traditional to advanced forms reflects humanity’s growing demand for materials capable of withstanding extreme conditions. While traditional ceramics (e.g., pottery, bricks) are derived from natural minerals like clays and feldspars, advanced ceramics emerged to address limitations in strength, thermal stability, and functionality. High-entropy ceramics (HECs) represent a groundbreaking subset of advanced ceramics, leveraging multi-cation disorder and entropy stabilization to achieve unprecedented properties.

## I.4. Definition of High-Entropy Ceramics

High-Entropy Ceramic is a type of advanced ceramic material that falls under the broader category of High-Entropy Materials (HEMs). High entropy systems can be defined through two primary approaches: the compositional definition and the thermodynamic (configurational entropy-based) definition [1].

### I.4.1. The compositional definition

High-entropy systems are characterized by the presence of four or more principal elements (*no less than four distinct cations or anions* ) in equimolar or near-equimolar ratios [6-10]. This multi-element composition is a defining feature, distinguishing high-entropy materials from traditional alloys or ceramics that typically contain one or two dominant elements.

The constituent elements are distributed in near-equiatomic ratios, with each element typically constituting between 5% and 35% of the total composition by atomic fraction [6-8]. This balanced distribution ensures that no single element dominates the structure, maximizing the configurational entropy of the system.

### I.4.2. Thermodynamic Definition of High-Entropy Systems (Based on Configurational Entropy)

Yeh et al. [8] defined high-entropy materials based on the configurational entropy ($\Delta S_{\text{conf}}$) calculated using the Boltzmann equation (Equation I.1):

$$\Delta S_{Conf} = -R(\sum_{i=1}^{N} x_i ln x_i) \qquad (1.I)$$

Where:

- $\Delta S_{\text{conf}}$ : Molar configurational entropy of the system (Jmol$^{-1}$K$^{-1}$).
- $x_i$ : Mole fraction of element *i*.
- $N$ : Total number of principal elements (or cations in ceramics).
- $R$ : Ideal gas constant (8.314 Jmol$^{-1}$K$^{-1}$).

A system is classified as high-entropy when $\Delta S_{\text{conf}} \geq 1.5R$, a threshold that promotes single-phase solid solution formation despite conflicting atomic/ionic sizes or bonding preferences [6,9]. Materials are broadly categorized by their configurational entropy values:

- **Low-entropy systems**: $\Delta S_{\text{conf}} < 1R$.
- **Medium-entropy systems**: $1R \leq \Delta S_{\text{conf}} < 1.5R$.
- **High-entropy systems**: $\Delta S_{\text{conf}} \geq 1.5R$ .

This entropy-driven stabilization mechanism underpins the design of advanced materials like high-entropy alloys (HEAs) and high-entropy oxide ceramics (HEOCs) [8,9].

## I.5. The Four Core Effects in High-Entropy Materials

The exceptional properties of high-entropy materials (HEMs), including high-entropy alloys (HEAs) and high-entropy ceramics (HECs), are attributed to four synergistic core effects as outlined in Murty et al. (2014) [11]. These effects collectively enhance stability, mechanical performance, and functional versatility:

### I.5.1. High-Entropy Effect

The increase in configurational entropy is a defining characteristic of high-entropy materials, playing a central role in their thermal stability. A significant rise in configurational entropy reduces the Gibbs free energy (Equation I.2), thereby promoting the formation of single-phase or fewer-phase solid solutions, particularly at elevated temperatures. Additionally, high entropy mitigates phase separation dynamics and reduces electronegativity differences between constituent elements [12.13].

$$\boldsymbol{G} = \boldsymbol{H} - TS \qquad \text{(I.2)}$$

Where:

- **G**: Gibbs free energy.
- **H**: Enthalpy.
- **S**: Entropy.
- **T**: Absolute temperature in Kelvin.

High entropy reduces the Gibbs free energy ($\Delta G_{mix}=\Delta H_{mix}-T\Delta S_{mix}$), favoring single phase formation even with positive mixing enthalpy ($\Delta H_{mix}>0$)

### I.5.2. Lattice Distortion Effect

High-entropy materials (HEMs) are characterized by a unique crystalline structure resulting from their crystalline lattice containing five or more elements with varying atomic sizes. This atomic size disparity leads to noticeable lattice distortions, where larger atoms displace neighboring atoms (inducing lattice compression), while smaller atoms create local vacancies (inducing lattice tension). This distortion generates internal lattice stress, increasing the system's total Gibbs free energy and directly impacting the material's physical properties.

Studies [14, 15] confirm that lattice distortion:

**A**. Enhances mechanical strengthening by impeding dislocation motion in the solid solution, thereby increasing deformation resistance [14].

**B**. Reduces electrical and thermal conductivity by increasing electron and phonon scattering due to lattice disorder, thereby negatively impacting the material's optoelectronic dynamics [15].

### I.5.3. Sluggish diffusion effect

The sluggish diffusion effect—one of the four core effects in high-entropy materials—proposes that atomic diffusion in multi-component systems (e.g., HEAs or HECs) is slower than in conventional alloys due to complex energy landscapes, high configurational entropy, and lattice distortion. While some studies attribute enhanced thermal stability and nanophase formation in HEAs to this effect, debates persist over its universality, as diffusion rates depend on temperature, crystal structure, and composition. In high-entropy ceramics, sluggish diffusion contributes to resistance against grain growth and phase separation at elevated temperatures, supporting their use in extreme environments [16-18].

### I.5.4. Cocktail effect

Before the discovery of high-entropy materials, in 2003, Ranganathan [19] published an article titled "Alloy Delights: Multimetallic Cocktails," in which he explained how multiple elements can produce unique properties when compared to a pure metal. Grain boundaries, phase boundaries, grain size distribution, and the distinctive properties of each phase contribute to the observed properties. The cocktail effect is one of the four core effects proposed to explain the unique properties of high-entropy materials, including high-entropy ceramics (HECs). It describes the synergistic interplay of multiple elements in a system, leading to unexpected or enhanced properties that cannot be predicted by the sum of individual elemental contributions [20].

High-entropy materials derive their exceptional properties from the interplay of four core mechanisms:

**1.Thermodynamic**: High configurational entropy stabilizes single-phase solid solutions by lowering Gibbs free energy.

**2.Kinetic**: Sluggish diffusion impedes phase separation and slows microstructural evolution.

**3.Structural**: Lattice distortion (from atomic size mismatch) enhances mechanical strength while reducing thermal/electrical conductivity.

**4.Synergistic**: The "cocktail effect" generates unexpected properties through multi-element interactions.

This integration of thermodynamic stability, kinetic sluggishness, and structural complexity enables high-entropy systems to achieve unprecedented performance in extreme environments.

## I.6. Classification of High-Entropy Materials

High-entropy materials are classified through multiple approaches in the scientific literature. The primary thermodynamic classification is based on configurational entropy: low-entropy ($\Delta S\_conf < 1R$), medium-entropy ($1R \leq \Delta S\_conf < 1.5R$), and high-entropy ($\Delta S\_conf \geq 1.5R$) systems. They can also be categorized by material class (high-entropy alloys, ceramics, or oxides), phase constitution (single-phase or multi-phase), crystal structure (FCC, BCC, HCP, or complex ceramic structures), application domain (structural or functional), and processing method (cast, powder metallurgy, additive manufactured, or thin film). This comprehensive classification framework enables researchers to select appropriate high-entropy systems for specific applications based on their entropy values, composition, structure, and desired properties [6].

## I.7. Classification of High-Entropy Materials

High-entropy oxides (HEOs) are an emerging class of advanced ceramic materials defined by their single-phase crystalline structure and incorporation of five or more principal metal cations in near-equiatomic proportions. Unlike traditional oxides, HEOs leverage configurational entropy to stabilize unconventional compositions, enabling unique properties and functionalitie [21,22].

## I.8. Pauling's Rules for Cation Selection in High-Entropy Oxides

Linus Pauling formulated five fundamental rules in 1929 to predict and rationalize the crystal structures of ionic compounds. These rules can be applied to high-entropy materials to enhance understanding of their crystalline behavior, with the rules ranked below in descending order of their influence on structural stability and physical properties [23,24].

### I.8.1. Radius Ratio Principle

A coordinated polyhedron of anions is formed about each cation, the cation-anion distance equaling the sum of their characteristic packing radii and the coordination polyhedron being determined by the radius ratio.

### I.8.2. Electrostatic Valence Balance

An ionic structure will be stable to the extent that the sum of the strengths of the electrostatic bonds that reach an anion equal the charge on that anion.

### I.8.3. Sharing of Polyhedron Elements

The sharing of edges and particularly faces by two anion polyhedra decreases the stability of an ionic structure.

### I.8.4. Rule for Multi-Valent Cations

In a crystal containing different cations, those of high valency and small coordination number tend not to share polyhedron elements with one another.

### I.8.5. Principle of Parsimony

The number of essentially different kinds of constituents in a crystal tends to be small.

## I.9. Crystalline Structures of High-Entropy Oxides

High-entropy oxides (HEOs) exhibit diverse crystalline structures that depend on their chemical composition and preparation conditions, despite their compositional complexity. The main structures are as follows:

### I.9.1. Rock-salt structure

It is also called B1 structure. Many halides and oxides crystallize in the cubic rock salt structure. In this structure the large anions are arranged in cubic close packing and all the octahedral interstices positions are filled with cations, as shown in Figure I.2. Oxides having this structure are MgO, CaO, SrO, BaO, CdO, MnO, FeO, CoO, and NiO. The coordination number is 6 for both cation and anion. For stability the radius ratio should be between 0.732 and 0.414, and the anion and cation valences must be the same. All the alkali halides except CsCl, CsBr, and CsI crystallize with this structure, as do the alkaline earth sulfides [25].

Generally, transition metal oxides crystallized in this structure exhibit distinctive properties like magnetism, electrochemical activity, and catalytic behavior. These properties are directly linked to the distribution of unique impurities and crystal defects within the rock-salt structure [26].

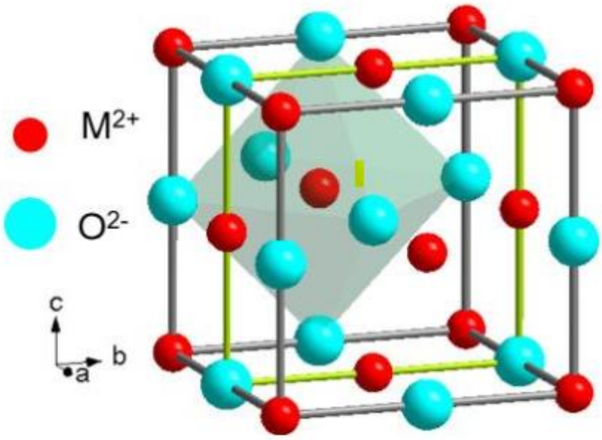

**Figure I.2:** The crystal structure of Rock-salt oxides.

### I.9.2. Spinel Structure

A number of oxides of the general formula $AB_2O_4$, such as magnesium aluminate (spinel), $MgAl_2O_4$ as shown in Figure I.3, have a cubic structure which can be viewed as a combination of the rock salt and zinc blende structures. The oxygen ions are in the face centered cubic close packing. The unit cell contains 32 oxygen ions, 16 octahedral cations, and 8 tetrahedral cations.

Two types of spinel occur. In the normal spinel the $A^{2+}$ ions are on tetrahedral sites and $B^{3+}$ ions are on octahedral sites. (This is the structure observed for $ZnFe_2O_4$, $MgAl_2O_4$, $FeAl_2O_4$, $NiAl_2O_4$, $MnAl_2O_4$ and $ZnAl_2O_4$). In the inverse spinel, the $A^{2+}$ ions and half the $B^{3+}$ ions are on octahedral sites; the other half of the $B^{3+}$ ions are on tetrahedral sites, $B(AB)O_4$. This is the more common structure and is observed for $FeMgFeO_4$, $FeTiFeO_4$, $Fe_3O_4$, $ZnSnZnO_4$, $FeNiFeO_4$, and many other ferrites of importance for their magnetic properties [27,28].

General Formula: $AB_2X_4$

Lattice: Face-Centered-Cubic

Z= 8 $MgAl_2O_4 = Mg_8Al_{16}O_{32}$

Atom positions: There are 56 atoms in the unit cell

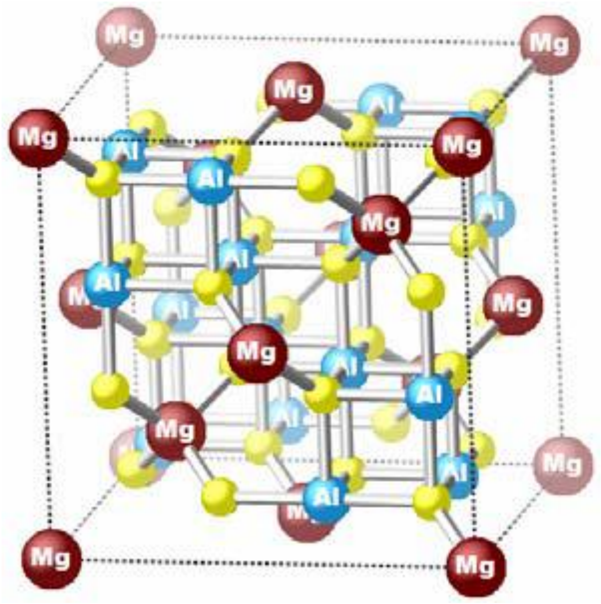

**Figure I.3:** The crystal structure of Spinel**.**

### I.9.3. Perovskite Structure

The name "perovskite" (Perovskite) originates from the natural mineral perovskite, $CaTiO_3$. Compounds of the perovskite type adopt the general formula $\mathbf{ABX_3}$, where:

**A** represents a cation with a large ionic radius, **B** denotes a cation with a smaller ionic radius, **X** is the anion.

In oxides, the formula simplifies to $ABO_3$. The ideal perovskite structure is cubic. In this arrangement:

The **A** cations and $O^{2-}$ anions together form a face-centered cubic (FCC) lattice. The **A** cations occupy the cube corners, while $O^{2-}$ ions reside at the centers of the cube faces [29,30].

This configuration creates a regular octahedral coordination environment at the center of which the B cation is located, as shown in Figure I.4.

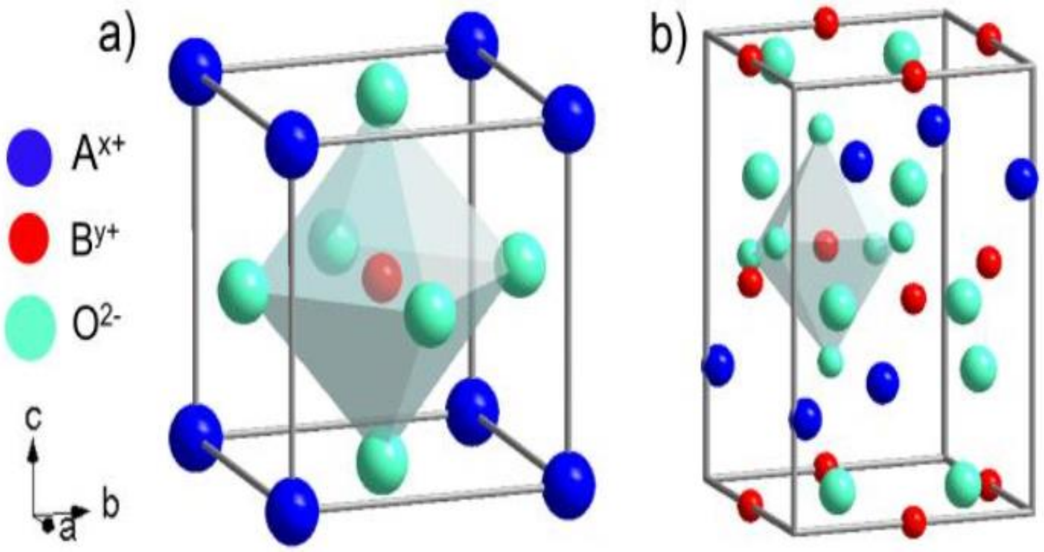

**Figure I.4:** Perovskite crystal structure (a) cubic structure (b) orthorhombic structure.

### I.9.4. Fluorite structure

The fluorite structure is named after the mineral fluorite ($CaF_2$) and follows the general formula $MX_2$ for compounds, where M represents cations and X represents anions. In oxides, this structure has the formula $MO_2$.

In the fluorite structure (as shown in Figure I.5): The anions (typically $O^{2-}$ in oxides) form a simple cubic lattice. Cations occupy all tetrahedral interstitial sites within this anion lattice.

The coordination number is 8 for cations (each surrounded by 8 anions) and 4 for anions (each surrounded by 4 cations). The structure features a face-centered cubic (FCC) arrangement of cations.

High-entropy oxides with fluorite structures are generally represented by formulas such as $(CeRE)O_{2-\delta}$ and $(\mathrm{HfZrCeM})O_{2-\delta}$, where: RE denotes rare-earth elements (e.g., La, Sm, Nd, Ho, Yb, Gd). M refers to transition or alkaline earth metals. δ is determined by the valence balance of cations [31].

Another important formula is $RE_2TM_2O_7$, where TM denotes transition metals such as Zr, Ti, Hf. This compound is characterized by its ability to crystallize in two different crystal structures, where the nature of the resulting crystal structure is determined by the ratio of the radius of the $RE^{3+}$ cation to the radius of the $TM^{4+}$ cation $[r(RE^{3+})/r(TM^{4+})]$. When this ratio ranges in the region of 1.46-1.78, the compound crystallizes in the pyrochlore structure, whereas when the ratio less than 1.46, the compound crystallizes in a disordered or defective fluorite structure [32].

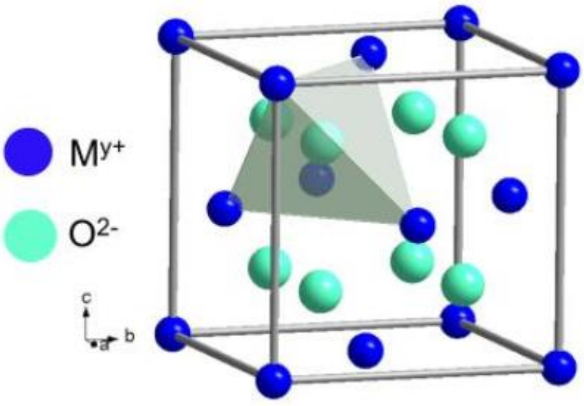

**Figure I.5:** The crystal structure of Fluorite.

### I.9.5. Pyrochlore structure

The pyrochlore structure is characterized by the formula $A_2B_2O_7$ and belongs to the space group $Fd\bar{3}m$ (No. 227). Here, A represents trivalent cations (rare earth elements) occupying the 16d crystallographic sites at coordinates (½, ½, ½), while tetravalent B cations (transition metals) occupy the 16c sites at coordinates (0, 0, 0). Oxygen ions are distributed over two distinct crystallographic sites:

-The 48f site at coordinates (x, 0.125, 0.125) (where x is a variable parameter).

-The 8b site at coordinates (0.375, 0.375, 0.375).

Natural oxygen vacancies are present at the 8a crystallographic sites at coordinates (0.125, 0.125, 0.125), creating a complex structure with ordered vacancies in the lattice [33], as shown in Figure I.6.

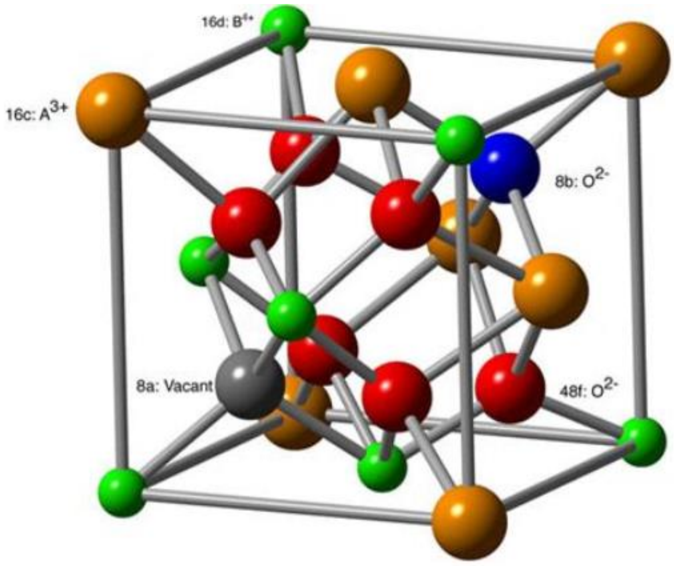

**Figure I.6:** The crystal structure of Pyrochlore.

Based on the crystallographic site distribution, coordination patterns depend on cation ionic radii and bonding. Large A-site cations exhibit 8-fold coordination, bonding with two 8b oxygen ions and six 48f oxygen ions. Smaller B-site cations show 6-fold coordination with 48f oxygen ions. Intrinsic oxygen vacancies at 8a sites, surrounded by four A-site cations [34], drive phase transformations that confer unique physical/chemical properties to pyrochlore

# I.10. Properties of High-Entropy Materials

## I.10.1. Mechanical Properties

High-entropy materials are characterized by a set of advanced mechanical properties that make them promising materials for engineering applications. These properties are determined by the complex interaction between the chemical composition, structure, and the preparation method used [35]. These fundamental properties include the following:

a. **High Strength and Hardness:** High-entropy materials exhibit exceptionally high strength and hardness [36, 37], giving them superior ability to resist deformation and fracture under various loads. This property is attributed to their complex crystal structure and strong bonding between their constituent elements, making them suitable for applications requiring high mechanical resistance.

b. **Outstanding Corrosion Resistance:** These compounds show exceptional corrosion resistance [38] thanks to their unique chemical composition and distinctive structural coherence. This robust cohesion allows for maintaining stability in aggressive and oxidative environments, ensuring a longer lifespan under harsh conditions.

c. **Superior Thermal Performance:** High-entropy compounds maintain stable mechanical performance over a wide range of high temperatures [39]. This thermal stability is attributed to the strength of atomic bonds and the regularity of the crystal structure, making them capable of withstanding thermal stresses without significant degradation in their basic properties.

d. **Resistance to Fatigue and Cyclic Loads:** As a result of their structural homogeneity and multi-element composition, these compounds exhibit remarkable resistance to mechanical fatigue. This property enables the materials to maintain their structural stability and mechanical performance under repeated cyclic loads for extended periods, making them ideal for applications requiring long-term stability and durability [35].

### I.10.2. Thermal Properties

Thermal conductivity is defined as a material's ability to conduct heat, which is determined by the transfer of phonons and electrons [40]. High-entropy materials generally possess low thermal conductivity due to the presence of multiple elements in their composition [41]. This complex composition induces lattice distortion, leading to phonon scattering and consequently a significant reduction in thermal conductivity.

High thermal stability and appropriate thermal expansion compatibility with the substrate are other features of thermal barrier coating ceramics [42]. Additionally, these materials typically exhibit excellent thermal stability [43], allowing them to maintain a consistent structure and performance even in high-temperature environments. This stability is attributed to the high-entropy effect, which prevents diffusion and phase separation processes that could weaken the material's properties.

### I.10.3. Electrical and Dielectric Properties

The multiple cations in high-entropy materials influence their electrical properties through lattice distortion and complex interactions between elements. These materials exhibit exceptional flexibility, as their conductivity can be tuned from insulators to conductors [44] by changing elements and their ratios. Some types show high electronic conductivity [45], while others exhibit excellent dielectric properties with very low conductivity [46], opening wide prospects for advanced technological applications.

### I.10.4. Magnetic Properties

Magnetism is a fundamental physical phenomenon arising from the movement of electric charges and the spin behavior of electrons, leading to a wide range of applications extending from traditional magnetic memory storage devices to advanced applications in spintronics, quantum sensing technologies, and emerging computing [47-49]. High-entropy materials emerge as an innovative class revolutionizing magnetic properties, as their high-entropy disordered nature perturbs and modifies traditional magnetic properties in unprecedented ways. These materials exhibit diverse magnetic properties including paramagnetism, ferromagnetism, antiferromagnetism, and ferrimagnetism, allowing for the design of materials with specific properties by controlling the types and ratios of components [50].

### I.10.5. Optical Properties

The optical properties of high-entropy oxides represent a vital research focus, not only for their future application potential but also for their fundamental role in exploring the electronic structure of these advanced materials. These optical properties gain exceptional importance when studying oxides doped with rare-earth elements, which exhibit unique capabilities in converting light wavelengths, qualifying them as promising candidates for enhancing the quantum efficiency of photovoltaic cells [51, 52].

## I.11. Synthesis methods

Synthesis methods play a pivotal role in the production of high-entropy ceramics, where the selection of the appropriate method requires consideration of phase stability, elemental distribution, and the final product's morphology. Synthesis methods are classified into: solid-state (e.g., ball milling for spherical sol), liquid (e.g., sol-gel and precipitation), and gaseous (e.g., sputtering deposition). In our study, we focused on solid-state methods (ball milling).

### I.11.1. Ball Milling (Solid-State Reaction)

Ball milling (Figure I.7) is a common technique for preparing high-entropy ceramics, where initial oxide powders are mixed with grinding balls to produce nanoparticles. This method is characterized by its simplicity and low cost, although the resulting particles may be irregularly shaped. Two types of reactions occur in it: solid-state reactions (for powders) and mechanochemical synthesis (for metal salts). The efficiency of the reaction depends on the melting point of the materials. When dealing with low melting point materials, diffusion between particles can occur during milling at room temperature [53]. For high melting point materials, ball milling is usually used only for mixing components, and diffusion primarily occurs during the subsequent heat treatment stage [54].

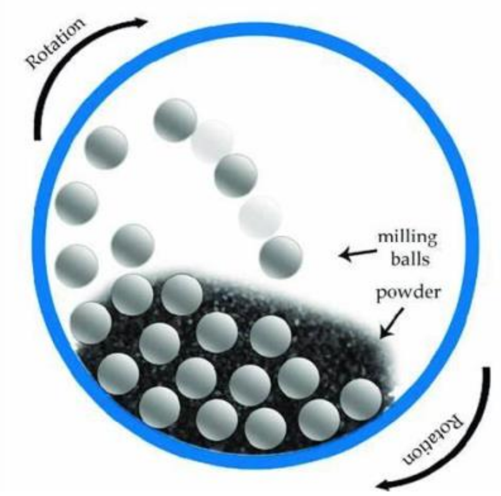

**Figure I.7:** Principle of Ball Mill technique.

### I.11.2. Sol-Gel Method

The sol-gel method (Figure I.8) is a versatile wet chemical synthesis technique for high-entropy ceramics (HECs), offering low cost, high-purity nanoparticles, and low-temperature processing. It involves reacting metal alkoxides (M–OR) with metal salts (e.g., nitrates or chlorides) to form the target oxide. Alkoxides are typically synthesized by dissolving metal salts in alcohol (not ethers), followed by hydrolysis and condensation to generate a sol-gel precursor. These reactions proceed in aqueous or organic solvents, enabling precise control over composition and nanostructure. The method is widely used to synthesize high-entropy oxides (HEOs) like (Mg,Co,Ni,Cu,Zn)O and fluorite-structured (Ce,La,Nd,Sm,Eu)$O_2$, which exhibit tailored properties for applications in energy storage and catalysis [55].

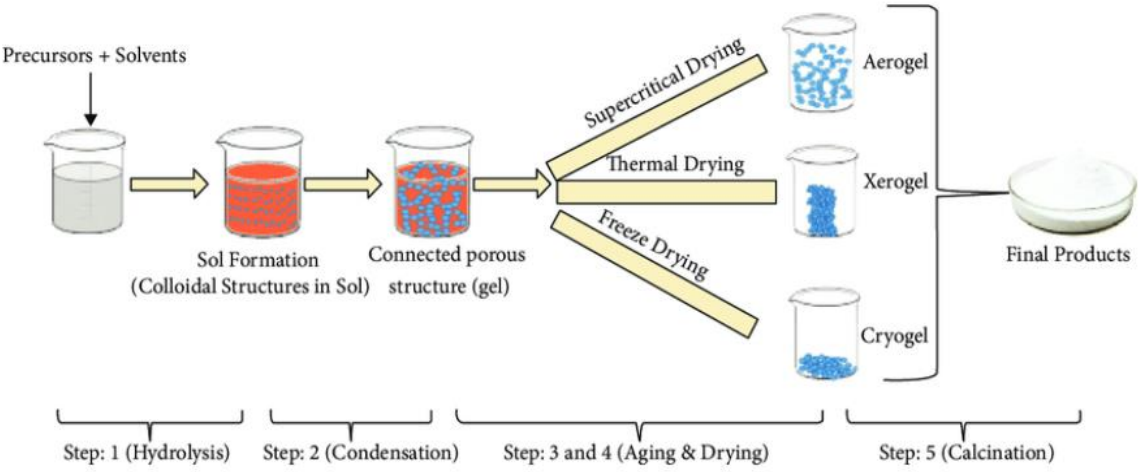

**Figure I.8**: Sol-Gel Method.

### I.11.3. Solution Combustion

The solution combustion method is used to synthesize high-entropy ceramic oxides through a reaction between a fuel (such as glycine), an oxidizer (usually metal nitrates), and oxygen, leading to the formation of oxides, water, and carbon dioxide. The sol is prepared by mixing hydrated metal nitrates with water and fuel, then it is dried to produce a gel which undergoes a thermal combustion process [56].

This method is characterized by efficiency, low cost, and applicability to a wide range of oxides and other ceramic materials. Sol-gel combustion is a similar approach that combines solution combustion and sol-gel techniques by using citric acid as both fuel and complexing agent [57].

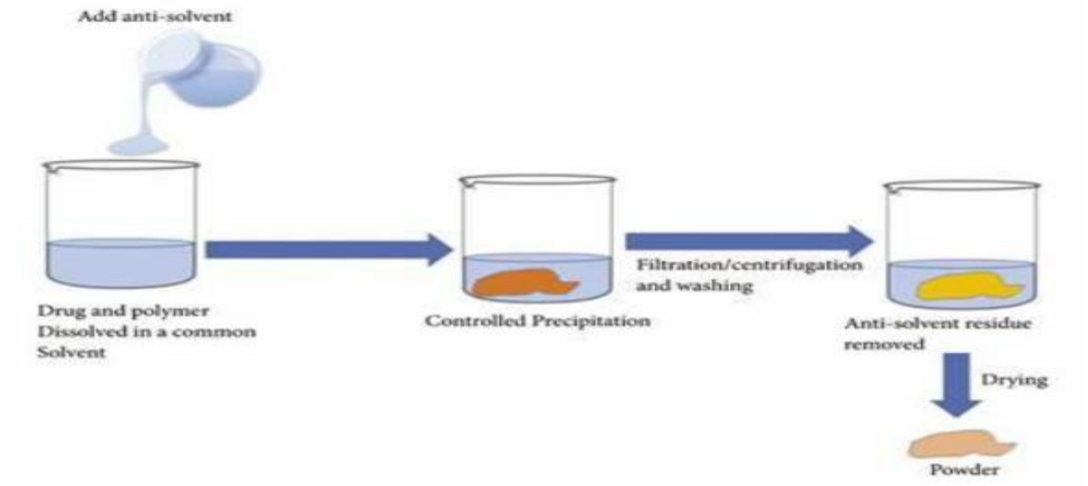

**Figure I.10:** Solution Combustion Method**.**

### I.11.4. Hydrothermal and Solvothermal Synthesis

Hydrothermal and solvothermal synthesis rely on the crystallization of materials in a sealed autoclave under high pressure and temperature, where water is used as a solvent in the hydrothermal method and an organic solvent in the solvothermal method. Particle morphology and sizes are controlled by several factors such as temperature, pH, and reactant concentration. These two methods are used to produce nanomaterials such as $TiO_2$ and graphene, and they are suitable for synthesizing high-entropy ceramics due to their simplicity compared to other methods. For example, Wang et al. were able to prepare $(CoCuFeMnNi)_3O_4$ with sizes up to 5 nm using solvothermal synthesis [58].

### I.11.5. Co-precipitation and Hydrothermal Treatment

Co-precipitation is commonly used to synthesize oxide or fluoride-based nanophosphors [59], where precursors (such as chlorides or nitrates) react with a base like NaOH in a suitable solvent. This method can be combined with hydrothermal treatment to enhance product homogeneity. These methods are used to synthesize some high-entropy oxides, such as (Mg,Co,Ni,Cu,Zn)O [60]. These approaches contribute to obtaining high-purity materials with advanced properties in applications.

## References

[1] E. Boaretto, X. Wu, J. Yuan, O. Bar-Yosef, V. Chu, Y. Pan, K. Liu, D. Cohen, T. Jiao, S. Li, Radiocarbon dating of charcoal and bone collagen associated with early pottery at Yuchanyan Cave, Hunan Province, China, Proceedings of the National Academy of Sciences 106(24) (2009) 9595-9600.

[2] R.B. Heimann, Classic and advanced ceramics: from fundamentals to applications, John Wiley & Sons2010.

[3] M.N. Rahaman, Ceramic processing and sintering, CRC press2017.

[4] S. Dorozhkin, Current state of bioceramics, J. Ceram. Sci. Technol 9(4) (2018) 353-370.

[5] A. Surendranathan, An introduction to ceramics and refractories, CRC Press2014.

[6] D. B Miracle & O. N. Senkov, 'A critical review of high entropy alloys and related concepts', Acta Materialia, vol. 122, pp. 448-511, Jan. 2017.

[7] B. Cantor, I. T. Chang, P. Knight, & A. J. B. Vincent, 'Microstructural development in equiatomic multicomponent alloys', Materials Science and Engineering: A, vol. 375, pp. 213-218, Jan. 2004.

[8] J. W. Yeh, S. K. Chen, S. J. Lin, J. Y. Gan, T. S. Chin, T. T. Shun & S. Y. Chang, 'Nanostructured high-entropy alloys with multiple principal elements: novel alloy design concepts and outcomes', Advanced Engineering Materials, vol. 6(5), pp. 299-303, Jan. 2004.

[9] M. Anandkumar & E. Trofimov, 'Synthesis, properties, and applications of high-entropy oxide ceramics: Current progress and future perspectives', Journal of Alloys and Compounds, vol. 960, pp. 170690, Jan. 2023.

[10] A. J. Wright, Q. Wang, C. Hu, Y.-T. Yeh, R. Chen, and J. Luo,’ Single-phase duodenary high-entropy fluorite/pyrochlore oxides with an order-disorder transition ‘ Acta Mater., vol. 211, pp. 116858, 2021.

[11] B. Murty, J. Yeh, and S. Ranganathan, *High-Entropy Alloys*, 1st (Butterworth-Heinemann, London, 2014), isbn: 9780128002513 (cit. on pp. 6–8, 10, 20, 48).

[12] X. Chang, M. Zeng, K. Liu, and L. Fu, ‘Phase Engineering of High-Entropy Alloys’, *Advanced Materials* vol.32, Issue14 , 2020.

[13] C. M.Rost, E.Sachet, T. Borman, A. Moballegh, E. C. Dickey, D.Hou, and J. P. Maria, ‘Entropy-stabilized oxides’. *Nature communications*, *6*(1), 8485.2015.

[14] O. N. Senkov, J. M. Scott, S. V. Senkova, D. B. Miracle, & C. F. Woodward, 'Microstructure and room temperature properties of a high-entropy TaNbHfZrTi alloy', Journal of alloys and compounds, vol. 509(20), pp. 6043-6048, 2011.

[15] Y. Zhang, High-Entropy Materials A Brief Introduction ,2019

[16] K.-Y. Tsai, M.-H. Tsai, and J.-W. Yeh, Acta Materialia, vol. 61, pp. 4887, Apr. 2013.

[17] M.-H. Tsai and J.-W. Yeh, Materials Research Letters, vol. 2, pp. 107, 2014.

[18] N. Qiu, H. Chen, Z. Yang, S. Sun, Y. Wang, & Y. Cui, 'A high entropy oxide (Mg0.2Co0.2Ni0.2Cu0.2Zn0.2O) with superior lithium storage performance', Journal of Alloys and Compounds, vol. 777, pp. 767-774, 2019.

[19] S. J. C. S. Ranganathan, Alloyed pleasures: Multimetallic cocktails. 2003.

[20] H. Xiang, Y. Xing… Y. Zhou, High-entropy ceramics: Present status, challenges, and a look forward, Journal of Advanced Ceramics, 10(3): 385–441. 2021.

[21] S. Jiang, T. Hu, J. Gild, N. Zhou, J. Nie, M. Qin, ... & J. Luo, 'A new class of high entropy perovskite oxides', Scripta Materialia, vol. 142, pp. 116-120, 2018.

[22] H. M. Princen, S. M. Post, & J. Twisk, 'Regulation of bile acid biosynthesis', Current Pharmaceutical Design, vol. 3(1), pp. 59-84, 1997.

[23] H. M. Princen, S. M. Post, J, Twisk, Regulation of bile acid biosynthesis, Current Pharmaceutical Design 3(1) (1997) 59-84.

[24] C. B. Carter, M. G. Norton, Ceramic materials: science and engineering (Vol. 716). Springer (2007).

[25] A. Sarkar, High Entropy Oxides: Structure and Properties (2020).

[26] A. Mao, H. Z. Xiang, Z. G. Zhang, K. Kuramoto, H. Yu, S. Ran, Solution combustion synthesis and magnetic property of rock-salt (Co0. 2Cu0. 2Mg0. 2Ni0. 2Zn0. 2) O high- entropy oxide nanocrystalline powder, Journal of Magnetism and Magnetic Materials (2019) 245-252.

[27] S. Liua, D. Nib, H.F Lic, S. C Jun, K. N. Hui, C.Y. Ouyang, Effect of cation substitution on pseudocapacitive performance of spinel cobaltite MCo2O4 (M = Mn, Ni, Cu, and Co), Journal of Materials Chemistry A.2018.

[28] Vl. Tsurkan , H. A. Krug von Nidda , J. Deisenhofer , P. Lunkenheimer , A. Loidl , On the complexity of spinels: Magnetic, electronic, and polar ground states, Physics Reports

Volume 926, Pages 1-86.2021.

[29] R. J. Tilley, Perovskites: structure-property relationships (John Wiley &amp; Sons, Inc., 2016), isbn: 9781118935668 (cit. on p. 75).

[30] N. J. M. S. Ramadass, $ABO_3$-type oxides—Their structure and properties—A bird&#39;s eye

view, Materials Science and Engineering 36(2) (1978) 231-239.

[31] C. Oses, C. Toher, S. Curtarolo, High-entropy ceramics, Nature Reviews Materials 5(4) (2020) 295-309.

[32] J. Wu, X. Wei, N. P. Padture, P. G, Klemens, M. Gell, E. García, M. I. Osendi, Low-thermal-conductivity rare-earth zirconates for potential thermal-barrier-coating applications, Journal of the American Ceramic Society 85(12) (2002) 3031-3035.

[33] M. A. Subramanian, G. Aravamudan, G. S. Rao, Oxide pyrochlores—a review, Progress in Solid State Chemistry 15(2) (1983) 55-143.

[34] Z. Teng, L. Zhu, Y. Tan, S. Zeng, Y. Xia, Y. Wang, H. Zhang, Synthesis and structures of high-entropy pyrochlore oxides, Journal of the European Ceramic Society 40(4) (2020) 1639-1643.

[35] Y. Wang, J. Zhang, T. Wu, G. Huang, Full-scale insight into high-entropy ceramics from basic concepts, synthesis technologies, structural characteristics, and properties to application prospects, Journal of Materials Research and Technology (2024) 398-430.

[36] W. Lu, L. Chen, W. Zhang, W. Su, Y. Wang, Y. Fu, Y. Zhou, Single-phase formation mechanical properties of (TiZrNbTaMo) C high-entropy ceramics: First-principles prediction and experimental study, Journal of the European Ceramic Society 42(5) (2022) 2021-2027.

[37] Y. Wang, T. Csanádi, H. Zhang, J. Dusza, M. J. Reece, Synthesis, microstructure, and mechanical properties of novel high entropy carbonitrides. Acta Materialia (2022) 117887.

[38] X. Wang, M. Cheng, G. Xiao, C. Wang, R. Qiao, F. Zhang, Z. Wang, Preparation and corrosion resistance of high-entropy disilicate (Y0. 25Yb0. 25Er0. 25Sc0. 25) 2Si2O7 ceramics. Corrosion Science (2021) 109786.

[39] T. Z. Ward, R. P. Wilkerson, B. L. Musicó, A. Foley, M. Brahlek, W. J. Weber, A. R. Mazza, High entropy ceramics for applications in extreme environments, Journal of Physics: Materials 7(2) (2024) 021001.

[40] R. Z. Zhang, M. J. Reece, Review of high entropy ceramics: design, synthesis, structure and properties, Journal of Materials Chemistry A 7(39) (2019) 22148-22162.

[41] D. Liu, B. Shi, L. Geng, Y. Wang, B. Xu, Y. Chen, High-entropy rare-earth zirconate ceramics with low thermal conductivity for advanced thermal-barrier coatings, Journal of Advanced Ceramics 11(6) (2022) 961-973.

[42] X. Wang, H. Xiang, X. Sun, J. Liu, F. Hou, Y. Zhou, Thermal properties of a prospective thermal barrier material: Yb3Al5O12, Journal of materials research 29(22) (2014) 2673-2681.

[43] S. Ye, J. Zhu, H. Wang, M. Li, Z. Huang, J. He, Phase evolution and thermal stability of novel high-entropy (Mo0. 2Nb0. 2Ta0. 2V0. 2W0. 2) Si2 ceramics. Journal of the European Ceramic Society 42(13) (2022) 5314-5322.

[44] H. Xie, J. Li, S. Yang, L. Wu, P. Li, X. Qi, Microstructures and dielectric properties of novel (La 0.2 Pr 0.2 Nd 0.2 Sm 0.2 Eu 0.2) 2 Ce 2 O 7 high entropy ceramics. Journal of Materials Science: Materials in Electronics (2021) 27860-27870.

[45] M. Kubisztal, Hopping conductivity and low-temperature magnetoresistance of high-entropy (Mn, Fe, Ni, Co, Zn) 3O4 polycrystalline ceramics, Ceramics International 49(11) (2023) 19442-19450.

[46] X. J. Chen, K. A. Khor, S. H. Chan, L. G. Yu, Influence of microstructure on the ionic conductivity of yttria-stabilized zirconia electrolyte, Materials Science and Engineering: A 335(1-2) (2002) 246-252.

[47] H. S. P. Wong, S. Salahuddin, Memory leads the way to better computing, Nature nanotechnology 10(3) (2015) 191-194.

[48] Q. L. He, T. L. Hughes, N. P. Armitage, Y. Tokura, K. L. Wang, Topological spintronics and magnetoelectronics, Nature materials 21(1) (2022) 15-23.

[49] G. Molnár, S. Rat, L. Salmon, W. Nicolazzi, A. Bousseksou, Spin crossover nanomaterials: from fundamental concepts to devices, Advanced Material 30(5) (2018) 1703862.

[50] S. Mallesh, J. S. Noh, Y. W. Nam, Structure and magnetic properties of (Mg1/6Zn1/6Mn1/6Co1/6Ni1/6Fe1/6) 3O4 nanocrystalline high-entropy oxide synthesized using a sol-gel auto combustion approach, Journal of Magnetism and Magnetic Materials (2022) 170108.

[51] J. de Wild, J. K. Rath, A. Meijerink, W. G. J. H. M. Van Sark, R. E. I. Schropp, Enhanced near-infrared response of a-Si: H solar cells with β-NaYF4: Yb3+ (18%), Er3+ (2%) upconversion phosphors, Solar energy materials and solar cells 94(12) (2010) 2395-2398.

[52] X. Huang, S. Han, W. Huang, X. Liu, Enhancing solar cell efficiency: the search for luminescent materials as spectral converters, Chemical Society Reviews 42(1) (2013)173- 201.

[53] D. Bérardan, S. Franger, D. Dragoe, A. K. Meena, N. Dragoe, Colossal dielectric constant in high entropy oxides, physica status solidi (RRL)–Rapid Research Letters 10(4) (2016) 328-333.

[54] J. Gild, M. Samiee, J. L. Braun, T. Harrington, H. Vega, P. E. Hopkins, J. Luo, High-entropy fluorite oxides, Journal of the European Ceramic Society 38(10) (2018) 3578-3584.

[55] A. Cestari, L. R. Avila, E. C. O. Nassor, P. F. S. Pereira, P. S. Calefi, K. J. Ciuffi, E. J. Nassar, Characterization of glass ionomer dental cements prepared by a non-hydrolytic sol- gel route, Materials Research 12(2) (2009) 139-143.

[56] F. T. Li, J. Ran, M. Jaroniec, S. Z. Qiao, Solution combustion synthesis of metal oxide nanomaterials for energy storage and conversion, Nanoscale 7(42) (2015) 17590-17610.

[57] T. Parida, A. Karati, K. Guruvidyathri, B. S. Murty, G. Markandeyulu, Novel rare-earth and transition metal-based entropy stabilized oxides with spinel structure, Scripta Materialia (2020) 513-517.

[58] D. Wang, Z. Liu, S. Du, Y. Zhang, H. Li, Z. Xiao, W. Chen, R. Chen, Y. Wang, Y. Zou, J. Mater. Chem. A Mater, Energy Sustain 7 (2019) 24211–24216.

[59] G.B. Nair, V.B. Pawade, S.J. Dhoble, in: B.A. Bhanvase, V.B. Pawade, S.J. Dhoble, S.H. Sonawane, M. Ashokkumar (Eds.), Nanomaterials for Green Energy, Elsevier Inc (2018) 411 431.

[60] M. Biesuz, L. Spiridigliozzi, G. Dell’Agli, M. Bortolotti, V. M. Sglavo, Synthesis and sintering of (Mg, Co, Ni, Cu, Zn) O entropy-stabilized oxides obtained by wet chemical methods, Journal of materials science 53(11) (2018) 8074-8085.

# Chapter Two

# Materials & Methods

## II.1. Introduction

Sample preparation represents an essential step in materials research. This chapter details the experimental protocols employed for synthesizing the ceramic powders and the characterization techniques utilized to investigate their properties. The experimental methodology encompasses several key analytical methods:

- Structural Characterization: X-ray Diffraction (XRD) provided the baseline for identifying crystalline phases and analyzing crystal structure.
- Thermal Property Analysis: Thermogravimetric Analysis (TGA) monitored weight changes during heating, indicating processes like decomposition or oxidation. Differential Thermal Analysis (DTA) complemented TGA by detecting enthalpic changes associated with reactions or phase transitions (e.g., melting, crystallization).
- Dimensional Stability: Dilatometry (DIL) measured the critical parameter of linear thermal expansion or contraction as a function of temperature.

## II.2. The Raw Materials

The chemical formula $Re_2(Zr_{0.5}Ti_{0.5})_2O_7$ represents a complex type of High-Entropy Oxide (HEO), and it is classified among High-Entropy Ceramics (HECs) The synthesis of $Re_2(Zr_{0.5}Ti_{0.5})_2O_7$ involves high-purity oxide precursors to ensure stoichiometric accuracy and minimize impurities. The selection of raw materials is based on their compatibility with the target composition and their role in forming the pyrochlore lattice.

High-purity oxide powders (all with a purity of 99.9%) were used as starting materials (Figure II.1):

**1.Rare-Earth Oxides (Re)** :

- $Nd_2O_3$ (neodymium oxide): Provides $Nd^{3+}$ ions (r = 1.109 Å, 8-fold coordination).
- $Sm_2O_3$ (samarium oxide): Supplies $Sm^{3+}$ ions (r = 1.079 Å)
- $La_2O_3$ (lanthanum oxide): Supplies $La^{3+}$ ions (r = 1.16 Å)
- $Yb_2O_3$ (ytterbium oxide): Supplies $Yb^{3+}$ ions (r = 1.008 Å)

**2.Transition Metal Oxides** :

- $ZrO_2$ (zirconium dioxide): Provides $Zr^{4+}$ ions (r = 0.72 Å, 6-fold coordination)
- $TiO_2$ (titanium dioxide): Supplies $Ti^{4+}$ ions (r = 0.605 Å)

The A-site incorporates four rare-earth cations with varying ionic radii (1.008–1.16 Å) to maximize configurational entropy while maintaining an average radius compatible with pyrochlore stability ($r(A) \approx 1.089$ Å). The B-site combines $Zr^{4+}$ and $Ti^{4+}$ to fine-tune lattice strain and thermal expansion behavior.

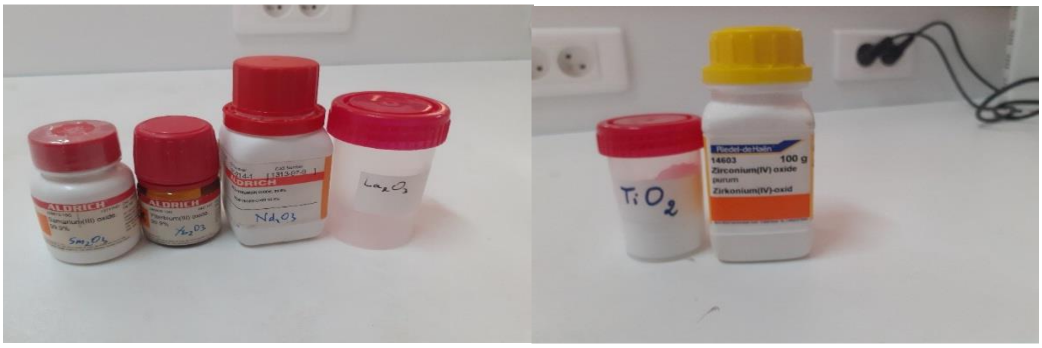

**Figure II.1**: the raw materials used.

## II.3. Preparation of Powders and Samples

Synthesis methods are of great importance in the growing fields of high-entropy ceramics, and selecting an appropriate synthesis route depends on various factors. $Re_2(Zr_{0.5}Ti_{0.5})_2O_7$ was synthesized in this study by the solid-state reaction method. The raw materials included neodymium(III) oxide ($Nd_2O_3$), samarium(III) oxide ($Sm_2O_3$), lanthanum(III) oxide ($La_2O_3$), ytterbium(III) oxide ($Yb_2O_3$), titanium(IV) dioxide and zirconium(IV) dioxide (also commonly referred to as zirconia ($ZrO_2$)) powders, all with a purity of 99.9% . The synthesis reaction was proposed according to the following equation:

$$Nd_2O_3 + Sm_2O_3 + La_2O_3 + Yb_2O_3 + ZrO_2 + TiO_2 + H_2O = (Nd_{0.25}Sm_{0.25}La_{0.25}Yb_{0.25})_2(Zr_{0.5}Ti_{0.5})_2O_7 + H_2O$$

The starting powders were accurately weighted based on the designed molar ratios (**15.17 wt.%** of $Nd_2O_3$, **15.73 wt.%** of $Sm_2O_3$, **14.69wt.%** of $La_2O_3$, **17.77 wt.%** of $Yb_2O_3$, **22.22 wt.%** of $ZrO_2$ and **14.41wt.%** of $TiO_2$). After completing the precise weighing of the raw materials, a mechanical mixing process with distilled water (2-3 ml) was carried out using a high-energy planetary ball mill

(Fritsch P6), equipped with zirconia balls (diameter of 10 mm), as shown in (**Figure II.2**). The milling process was conducted at room temperature at a speed of 300 r·min$^{-1}$ for 2 hours, while maintaining a milling ball-to-powder ratio of 10:1 to ensure the efficiency of the mixing process. After milling, the milled mixture was dried in an oven at 120°C for 24 hours, to remove adsorbed moisture and ensure obtaining a dry, fine, and homogeneous powder in preparation for the thermal sintering stage

**Figure II.2**: Planetary ball mill (Fritch P6) and zirconia balls

After preparing the homogeneous powders, cylindrical ceramic samples were formed using a **uniaxial hydrostatic press**, as shown in Figure (II.3). We took weighted amounts of these powders and placed them in a steel mold, then pressed them under a pressure of 250 MPa for a sufficient time to allow pressure distribution inside the mold, resulting in the production of cylindrical samples with a diameter of 10 mm.

To improve the physical and mechanical properties of the ceramic and to obtain ceramics with high density and good crystallization, the compacted samples underwent heat treatment inside a **Nabertherm** electric furnace at temperatures ranging between 1400-1500°C for 4-8 hours. A controlled heating and cooling rate were maintained to avoid cracking of the samples during the expulsion of. 1. Figure II.4 shows the flowchart for $(Nd_{0.25}Sm_{0.25}La_{0.25}Yb_{0.25})_2(Zr_{0.5}Ti_{0.5})_2O_7$ preparation process.

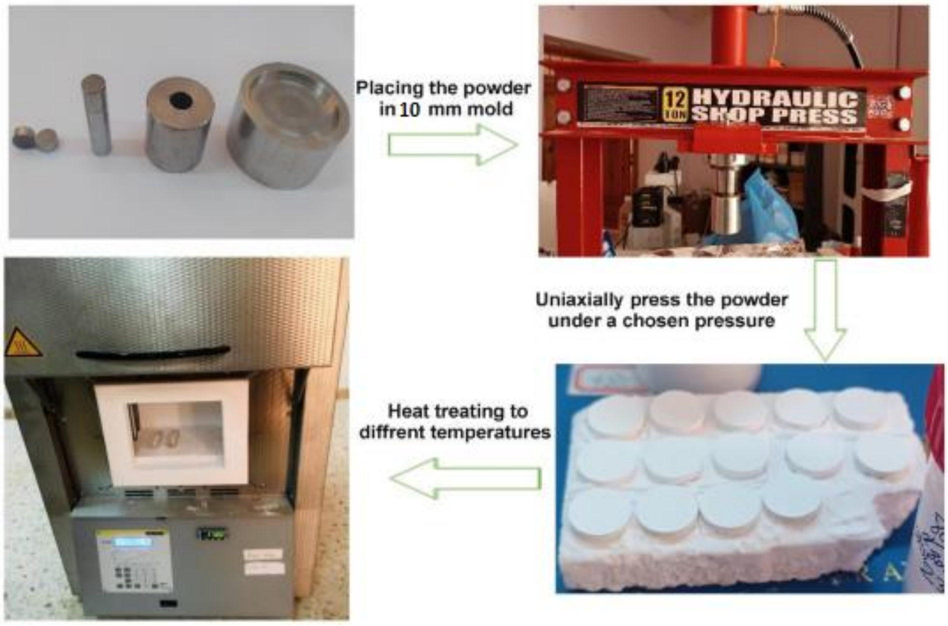

**Figure II.3**: The process of molding and sintering samples.

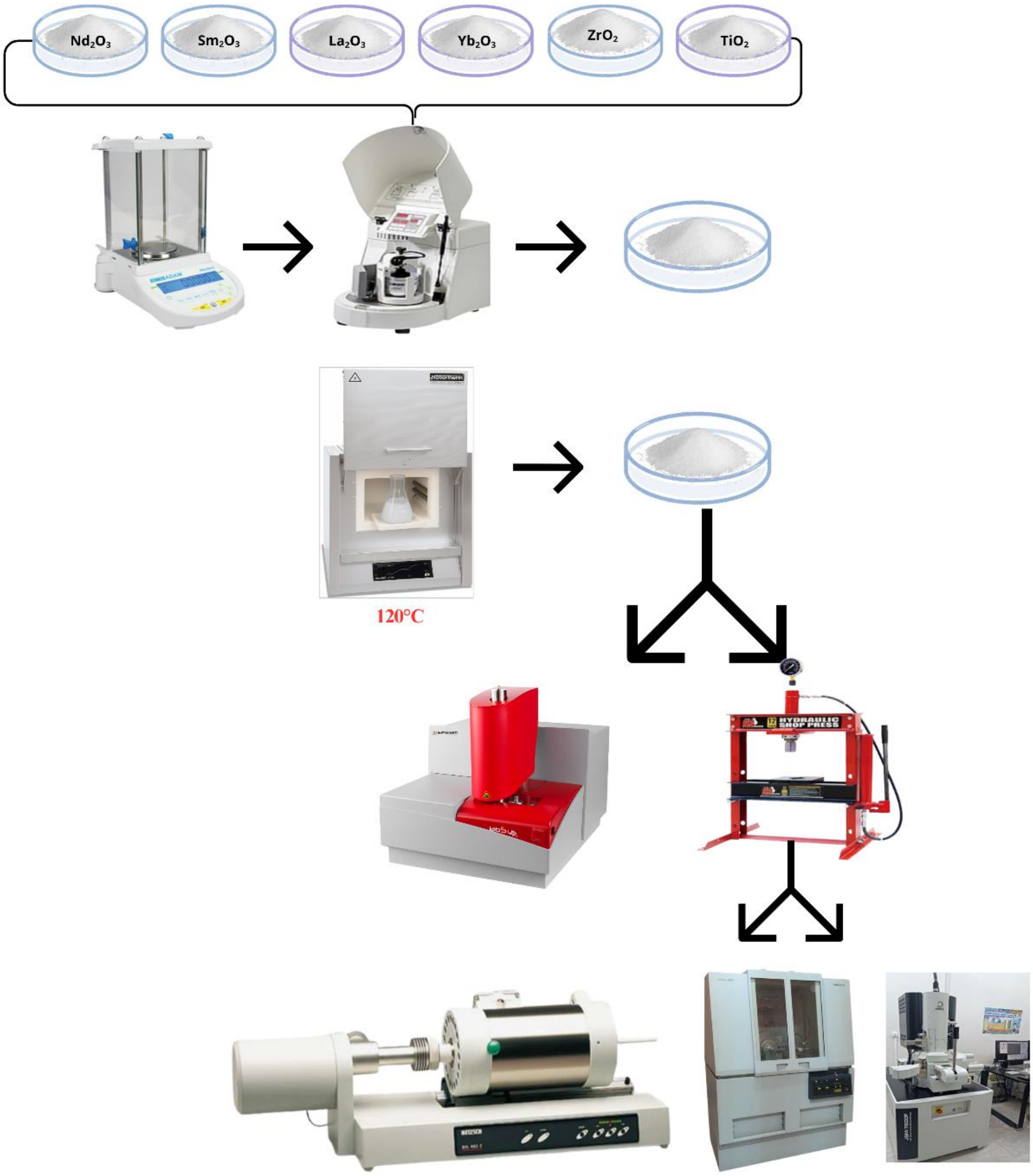

**Figure II.4**: the flowchart of preparation process.

## II.4. Characterization techniques and equipment

### II.4.1. Thermal Analysis and Calorimetry (TGA/DSC/DTA)

Thermal analysis (TA) techniques such as thermogravimetry (TG), differential thermogravimetry (DTG), differential scanning calorimetry (DSC), and differential thermal analysis (DTA) are widely employed to characterize material properties, including thermal capacity, mass changes, enthalpy, and thermal expansion.

Among these, thermogravimetry (TG) measures the mass change of a sample (e.g., ceramics, metals, polymers) as a function of temperature or time under controlled conditions, including specific environments (using various gases like nitrogen, helium, and air), with typical sample masses exceeding 25 mg and heating rates ranging from 1–50 °C/min, providing valuable information on evaporation rates and decomposition reactions. Complementary to TG, differential thermogravimetry (DTG) represents the first derivative of the TG curve (mass loss rate vs. temperature/time), highlighting subtle mass changes and enabling precise identification of decomposition steps and reaction temperatures. Differential Scanning Calorimetry (DSC) quantifies the heat flow required to maintain the sample and reference at the same temperature during heating, cooling, or isothermal conditions, with the term "differential" referring to the measurement with respect to a standard reference, as illustrated in Figure II.5, primarily measuring heat flow as a function of temperature and time to identify different phase transitions, where endothermic transitions (negative temperature differential) appear as downward peaks while exothermic transitions point upward.

Differential Thermal Analysis (DTA) works on a similar principle to DSC but measures the temperature difference (ΔT) between the sample and an inert reference as a function of time or temperature, with the signal typically expressed in microvolts (μV), showing peaks that correspond to endothermic or exothermic events.

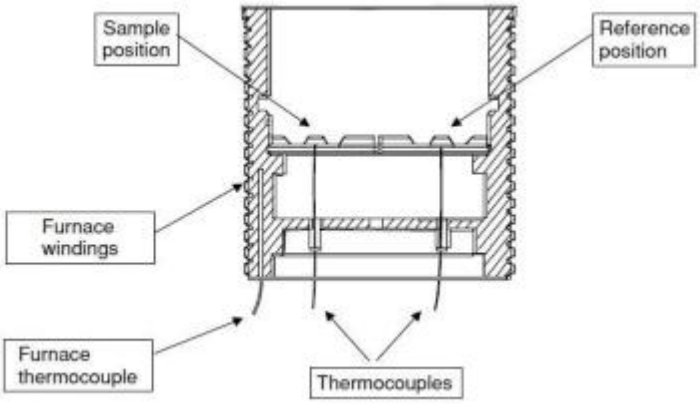

**Figure II.5**: Diagram of a heat flux DSC system.

To identify and determine the phase transformation for the synthesized powders, thermal analysis using LABSYS Evo DTA/DSC-TG SETARAM 1600 °C equipment (TG/DTG and DSC) shown in Figure II.6 was used.

**Figure II.6**: LABSYS Evo DTA/DSC-TG SETARAM 1600 °C equipment (univ of M’sila)

.

### II.4.2. Dilatometry (DL)

Dilatometry is a technique used to measure the thermal expansion of materials by observing the length change of a sample as it is subjected to controlled temperature variations. The dilatometry equipment used is shown in Figure II.7.

The method involves using a pushrod to transmit the displacement of the expanding sample to a Linear Differential Variable Transformer (LVDT), which converts the mechanical movement into a voltage signal that is recorded and processed by specialized software. This allows precise monitoring of the sample's elongation as a function of temperature. The equipment used in dilatometry includes a dilatometer apparatus equipped with an LVDT, a sample holder, and a furnace for heating the sample, as shown in Figure II.8.

Netzsch DIL 402 ES dilatometer system also incorporates a Thermal Analysis System Controller (TASC) to connect the dilatometer to the measurement software, a coolant system to maintain the LVDT at a constant temperature (25°C), and a vacuum pump for removing oxidizing gases.

The entire system is managed through a CPU that logs and processes the collected data. The CTE OF prepared samples were analyzed using a Netzsch DIL 402 ES dilatometer in the range of [100- 1200 °C].

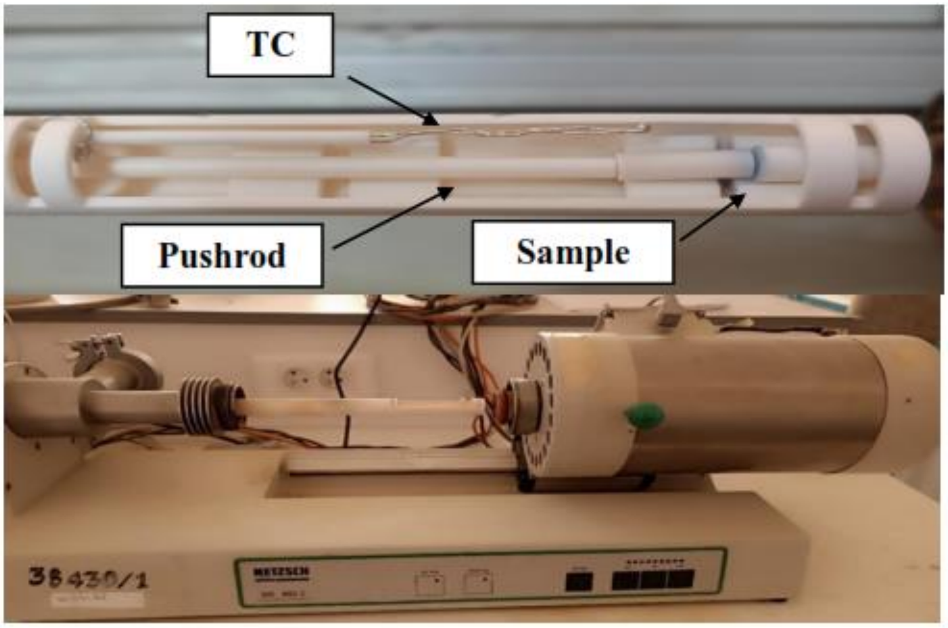

**Figure II.7**: Netzsch DIL 402 C dilatometry (DL) equipment and close-up view of the sample holder (univ of M’sila).

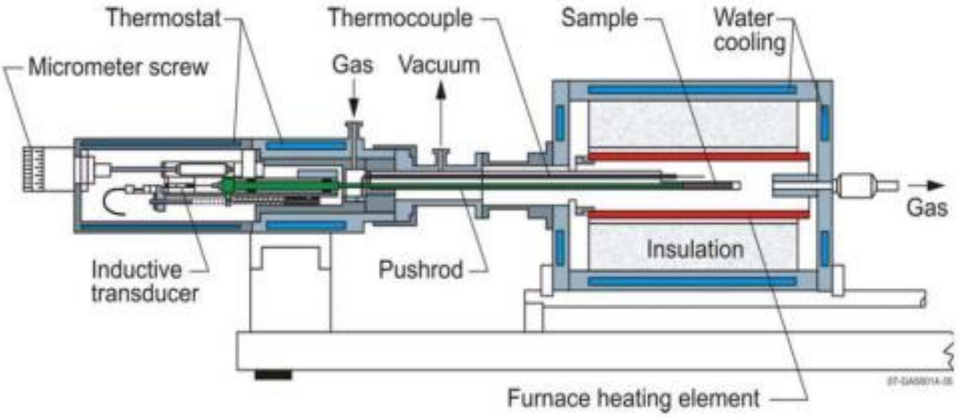

**Figure II.8**: Schematic of dilatometer in horizontal configuration.

### II.4.3. X-ray Diffraction (XRD)

X-ray diffraction is a non-destructive means of determining crystalline structure, studying phase equilibria, determining the orientation of crystals, and measuring particle size. The technique of X ray diffractions at the beginning was linked to the German physicist Von Laue's (1879-1960) discovery in 1912, which stated that x-rays diffract by means in crystals if the interatomic distance in crystals were equal to the wavelength of x-rays electromagnetic waves, later on, an English physicist W. L. Bragg expressed necessary conditions for diffraction to occur and formulated what is known today as the Bragg's law (Eq. 1):

$$\mathbf{2}.\boldsymbol{d}\sin\boldsymbol{\theta} = \mathbf{n\lambda} \qquad (\mathbf{1})$$

Where**:**

θ: is the angle between the incident ray and the scattering planes

d: the spacing between the planes in the atomic lattice

n: is an integer determined by the diffraction order

λ: X-ray wavelength.

In this research, we utilized X-ray analysis equipment to perform qualitative analysis of the samples before and after any treatment. The analysis was conducted using the Xpert Pro Panalytical instrument available in laboratory at M'sila University, as shown in Figure (II.9), which operates at room temperature. It operates with a voltage of 40 kV and a current intensity of 30 mA. This instrument emits a monochromatic X-ray beam with a wavelength of (λ = 1.5418 Å) from a Cu(Kα) source, which falls on the sample and then diffracts after interacting with the crystalline phases according to Bragg's Law.

**Figure II.9**: X-ray diffractometer (X'Pert Pro, Analytical) (univ of M'sila).

### II.4.4. Scanning Electron Microscopy (SEM)

Scanning electron microscopy (SEM) is a versatile technique used to obtain high-resolution and detailed imagery for selected sample surfaces compared to optical microscopy. Such type of analysis uses a focused accelerated electron (1 KeV- 30 KeV) beam (1- 20 nm diameter) to scan and then create an image of the specimen surface, as shown in Figure II.10. The produced signals collected using specialized detectors (detectors such as backscattered electron detector (BSD) and secondary electron detector (SED)) are used to provide high-resolution imagery. The signals detected with the aid of an external computer help in forming images and collecting various information like the surface's elements composition and topography.

This thesis used the SEM (QUANTA 250 FEG-FEI) shown in Figure II.11 to study the microstructure of samples.

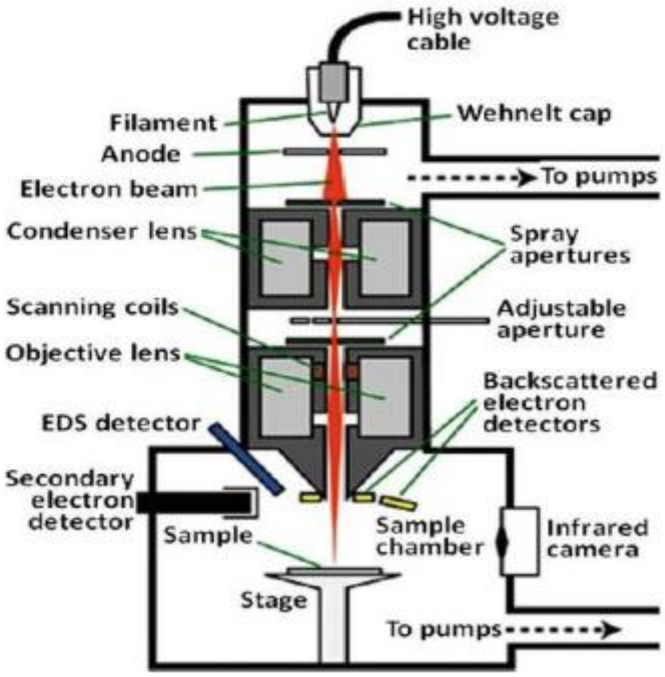

**Figure II.10**: Scanning electron microscopy (SEM) schematic with other detectors.

### II.4.5. Energy Dispersive Spectroscopy (EDS)

Understanding that the unique electrons transition between different energy levels inside different element atoms can be used to characterize materials. EDS or EDX can be coupled with scanning electron microscopy (SEM), EDS measures the energy of the characteristic X-ray spectrum emitted by the material, these x-rays are produced when primary focused electron beam (sufficient to knock electrons off from inner layer in atoms) bombard the sample. To convert the x-ray energy to voltage signals, a detector is used; by displaying selected x-ray line intensity, the chemical composition and elements distribution of the sample can be determined.

**Figure II.11**: Scanning electron microscopy (SEM) combined with Energy Dispersive Spectroscopy (EDS) (univ of Bejaia).

# Chapter Three

# Results & Discussion

## III.1. Crystal Structure Analysis of $A_2B_2O_7$ Oxides: Pyrochlore vs. Defect Fluorite

The formation of a stable $A_2B_2O_7$-type pyrochlore structure is closely determined by the ionic radius ratio between the A-site and B-site cations, as described by the Shannon–Prewitt effective ionic radii [1]. For the pyrochlore structure to form, the ratio r(A)/r(B) [where A is in eightfold coordination (VIII-fold coordination) and B is in sixfold (VI-fold coordination)] typically falls within the range of 1.46 to 1.78 [2]. This geometrical constraint ensures the formation of a long-range ordered superstructure, distinct from the disordered defect fluorite phase.

In the case of the $(Nd_{0.25}Sm_{0.25}La_{0.25}Yb_{0.25})_2(Zr_{0.5}Ti_{0.5})_2O_7$ system:

a. A-site cations (VIII-fold coordination):

- $La^{3+}$: 1.16 Å
- $Nd^{3+}$: 1.109 Å
- $Sm^{3+}$: 1.079 Å
- $Yb^{3+}$:1.008Å
  - ➢ Average r(A) = (1.16 + 1.109 + 1.079 + 1.008) / 4 = 1.089 Å

b. B-site cations (VI-fold coordination):

- $Zr^{4+}$: 0.72 Å
- $Ti^{4+}$:0.605Å
  - ➢ Average r(B) = (0.72 + 0.605) / 2 = 0.6625 Å

Thus, the ionic radius ratio is:

$$r(A)/r(B) = 1.089 / 0.6625 \approx \mathbf{1.64}$$

This value clearly falls within the stability range of the pyrochlore structure ($1.46 < r(A)/r(B) < 1.78$), indicating that the system has a strong tendency to crystallize in an ordered pyrochlore phase.

Additionally, the compositional complexity due to multiple rare-earth and transition-metal cations increases the configurational entropy, which enhances structural stability and may influence functional properties such as oxygen vacancy concentration, radiation tolerance, and thermal conductivity. Therefore, $(Nd_{0.25}Sm_{0.25}La_{0.25}Yb_{0.25})_2(Zr_{0.5}Ti_{0.5})_2O_7$ can be regarded as a promising high-entropy pyrochlore ceramic with potential for advanced energy and environmental applications.

## III.2. Thermogravimetry (TG/DTG), Differential thermal analysis (DTA)

To investigate the thermal stability, mass loss behavior, and phase transformation characteristics occurring in $A_2B_2O_7$ Oxides powder during heat treatment, thermogravimetric analysis (TG) and its derivative were performed on $(Nd_{0.25}Sm_{0.25}La_{0.25}Yb_{0.25})_2(Zr_{0.5}Ti_{0.5})_2O_7$ powder at a heating rate of 30 °C/min under an argon gas flow of 40 mL/min. Figure III.1 shows the TG and dTG curves as a function of temperature from room temperature up to 1400 °C. These curves reveal multi-step mass loss processes. In the low-temperature range (ambient to ~300 °C), the first mass loss (approximately 0.2 wt%) corresponds to an endothermic peak observed near 100–200 °C, which is attributed to the removal of adsorbed water introduced during the mixing of oxides with distilled water in the synthesis process. In the temperature range (200–700 °C), two endothermic peaks are observed in the dTG curve, accompanied by an additional mass loss of approximately 0.6 wt% in the TG curve. This behavior is attributed to the thermal decomposition of residual precursor compounds, such as rare-earth hydroxides or carbonates, which may have formed during the synthesis or subsequent storage due to atmospheric moisture or $CO_2$ adsorption. Specifically, hydroxides like $RE(OH)_3$ decompose to $RE_2O_3$ with the release of water vapor, while carbonates such as $RE_2(CO_3)_3$ decompose to oxides with the liberation of $CO_2$ gas [3]. When $Sm_2O_3$ or $La_2O_3$ is used as a precursor, it may react with atmospheric $CO_2$ , or it may partially hydrolyze during the mixing step with distilled water (for example: during wet milling or mixing with distilled water, the oxide undergoes partial hydrolysis to form $Sm(OH)_3$, as described by the reaction: $Sm_2O_3 + 3H_2O \rightarrow 2Sm(OH)_3$), forming $Sm_2(CO_3)_3$ or $Sm(OH)_3$. These compounds thermally decompose in the 400-800°C range, explaining both the two endothermic peaks and corresponding mass loss in this region. The decomposition follows the reaction: $Sm_2(CO_3)_3 \rightarrow Sm_2O_3 + 3CO_2\uparrow$, or $2Sm(OH)_3 \rightarrow Sm_2O_3 + 3H_2O\uparrow$ consistent with the observed 0.6% mass loss .

This phenomenon has been well-documented in rare-earth oxide systems, particularly for Sm, La-containing compositions. A subsequent mass loss event (<0.4 wt%), detected at higher temperatures (700–850°C) is associated with final decarbonation of stable oxycarbonates ($RE_2O_2CO_3 \rightarrow RE_2O_3 + CO_2$) and initiation of the solid-state reaction ($RE_2O_3 + ZrO_2 + TiO_2 \rightarrow RE_2(Zr,Ti)_2O_7$) [3,4].

Beyond 850°C, the TG curve stabilizes, indicating the formation of a thermally stable oxide phase. The stability of the structure at elevated temperatures, along with the absence of further mass loss, suggests the formation of a single-phase pyrochlore.

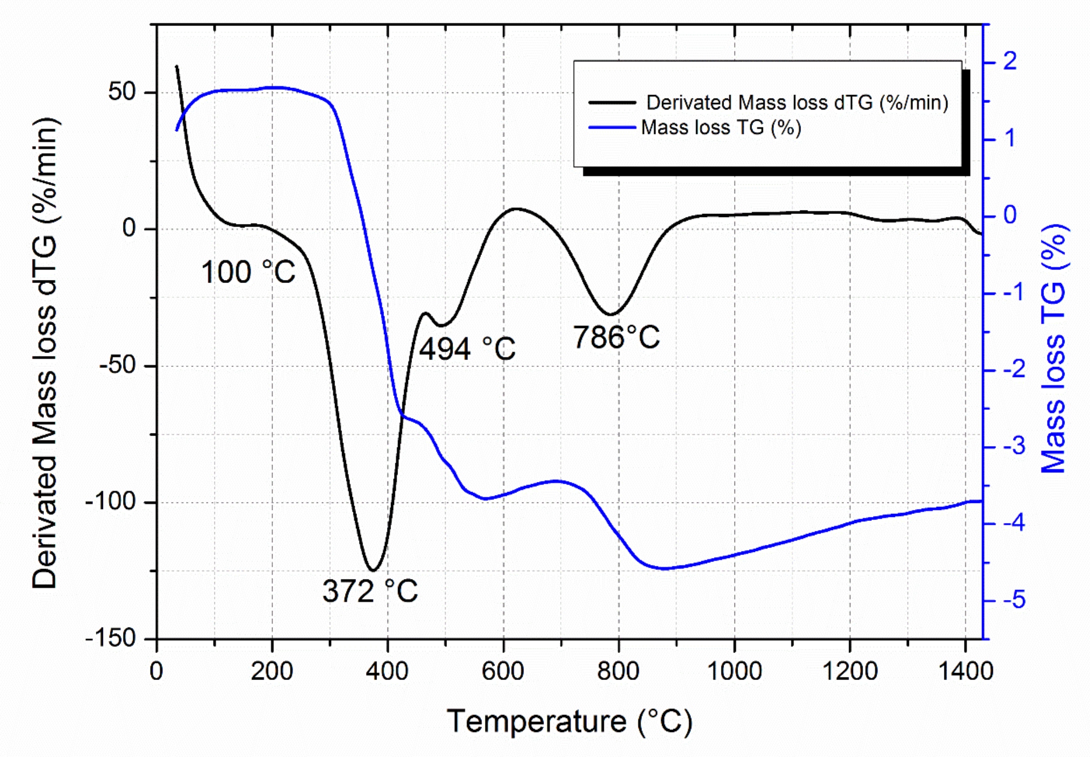

**Figure III.1**: TG and dTG curves for $(Nd_{0.25}Sm_{0.25}Ho_{0.25}Yb_{0.25})_2Zr_2O_7$ powder heated at 30 °C/min up to 1400 °C.

The DTA curve (Figure III.2) provides essential information about the thermal events associated with physical and chemical transformations occurring in the $(Nd_{0.25}Sm_{0.25}La_{0.25}Yb_{0.25})_2(Zr_{0.5}Ti_{0.5})_2O_7$ system during heating. Multiple endothermic and exothermic peaks were observed, relating well with the mass loss features identified in the TG and dTG curves.

- The first endothermic peak, observed between 100°C and 200°C, is attributed to the evaporation of adsorbed water introduced during the wet synthesis involving distilled water.
- The second endothermic peak, occurring in the 200–400°C range, corresponds to the decomposition of rare-earth hydroxides such as $Sm(OH)_3$ and $La(OH)_3$, formed by partial hydrolysis of $Sm_2O_3$ or $La_2O_3$ during mixing with water.
- A third endothermic peak, detected between 400°C and 700°C, is associated with the thermal decomposition of rare-earth carbonates, e.g., $Sm_2(CO_3)_3$, releasing $CO_2$ gas.
- An additional endothermic event, observed between 700°C and 850°C, is attributed to the decarbonation of stable oxycarbonates ($RE_2O_2CO_3 \rightarrow RE_2O_3 + CO_2$), alongside the onset of solid-state reactions between $RE_2O_3$, $ZrO_2$, and $TiO_2$, which lead to the formation of the final $A_2B_2O_7$ oxide phase.
- Notably, the DTA curve also exhibits two broad exothermic peaks centered around 1100 °C and 1400 °C. The first transformation is recorded in the thermal range of 1091°C to 1134°C, characterized by an endothermic peak in the Differential Thermal Analysis (DTA) curve with no associated mass change in the Thermogravimetry (TG) curve. The maximum transformation rate occurs at 1115°C. This event is attributed to a solid-solid phase transition in the zirconium oxide ($ZrO_2$) structure—a material known for its temperature-dependent polymorphic behavior. The transition is identified as the transformation from the monoclinic phase to the tetragonal phase, a well-documented phenomenon in scientific literature [5].
- The last exothermic peak at 1400°C likely reflect crystallization processes, structural rearrangements, or grain growth associated with the formation or stabilization of the pyrochlore phase at elevated temperatures.

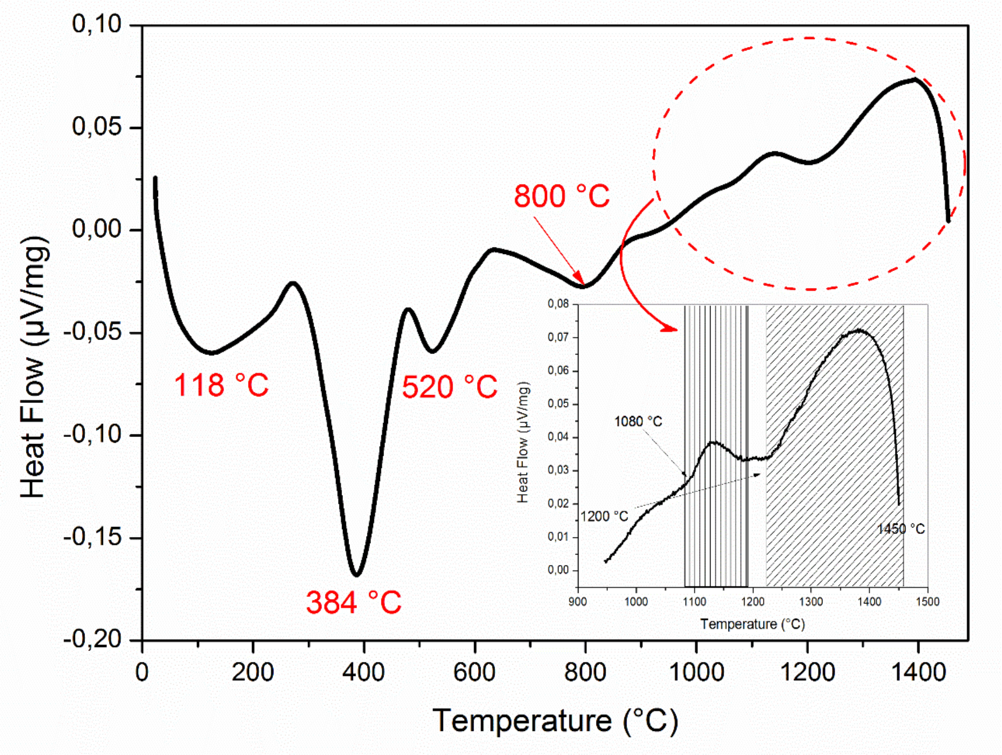

**Figure III.2**: DTA curve for $(Nd_{0.25}Sm_{0.25}Ho_{0.25}Yb_{0.25})_2Zr_2O_7$ powder heated at 30 °C/min up to 1400 °C.

## III.3. X-ray diffraction analysis (XRD)

A series of thermal treatments were performed on the $(Sm, Nd, La, Yb)_2(Ti_{0.5}, Zr_{0.5})_2O_7$ compound using Differential Thermal Analysis (DTA) at different temperatures 1080 °C, 1200 °C, and 1450 °C to investigate the effect of temperature on phase formation and structural evolution. Following each thermal treatment, the sample was subjected to X-ray diffraction (XRD) analysis (Figure III.3) to identify the resulting crystalline phases. These patterns are compared with the standard reference patterns of $Sm_2Zr_2O_7$ pyrochlore type (PDF#00-024-1012) with space group $Fd\bar{3}m$ (No. 227).

At a temperature of 1080 °C and according to phase identification using HighScore Plus software, the elemental distribution indicates that the rare-earth cations (Sm, Nd, La, Yb) remain segregated at the A-site, while Ti and Zr occupy the B-site. This suggests that the complete formation of a homogeneous $A_2B_2O_7$ solid solution (pyrochlore) has not yet been achieved at this temperature. At 1200 °C, the disappearance of some precursor-related signals and the emergence of sharper diffraction peaks indicate the onset of a more advanced crystallization stage. This temperature marks a significant step in the formation of a thermodynamically stable phase. Specifically, the partial disappearance of distinct signals corresponding to individual rare-earth or transition metal oxides suggests that the constituent elements have begun to react more completely and integrate into a single, ordered lattice structure. Further heating to 1400 °C intensified the crystallization process, resulting in the elimination of most secondary phases and the development of a well-defined and thermally stable structure (pyrochlore-type configuration). These results emphasize the critical role of temperature in governing the structural development of high-entropy oxides and demonstrate a gradual evolution toward a thermodynamically stable phase.

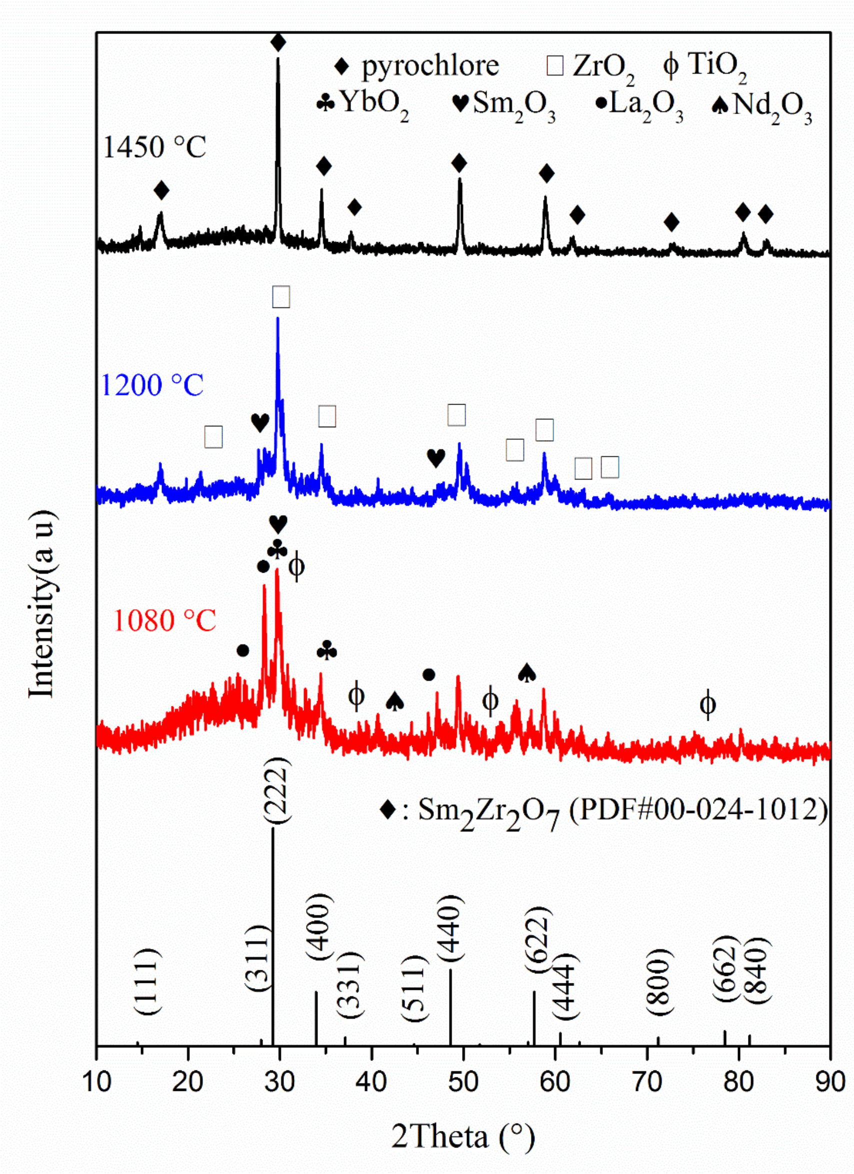

**Figure III.3**: XRD patterns of $(Nd_{0.25}Sm_{0.25}Ho_{0.25}Yb_{0.25})_2Zr_2O_7$ ceramics sintered at 1080°C, 1200°C and 1450°C, compared with the standard reference patterns of $Sm_2Zr_2O_7$ (PDF#00-024-1012).

## III.4. Crystal Structure Visualization Using VESTA

The crystal structure of the $(Sm,Nd,La,Yb)_2(Ti_{0.5},Zr_{0.5})_2O_7$ compound was modeled using the VESTA software, based on structural parameters obtained from crystallographic databases or previous XRD results. The model (as presented in Figure III.4) revealed that the compound crystallizes in the typical pyrochlore structure, which belongs to the cubic crystal system (with space group $Fd\bar{3}m$ (No. 227). The visualization clearly showed the ordered arrangement of rare-earth cations ($RE^{3+}$) at the A-sites and $Ti^{4+}/Zr^{4+}$ cations at the B-sites, surrounded by oxygen atoms forming a three-dimensional, stable network. VESTA allowed for a detailed visualization of the atomic positions and coordination environments, including the characteristic vacancies and distortions associated with the pyrochlore structure. This structural representation enhances the understanding of the material's atomic-scale architecture and supports the interpretation of its physical properties, such as thermal stability, thermal expansion, and potential ionic conductivity.

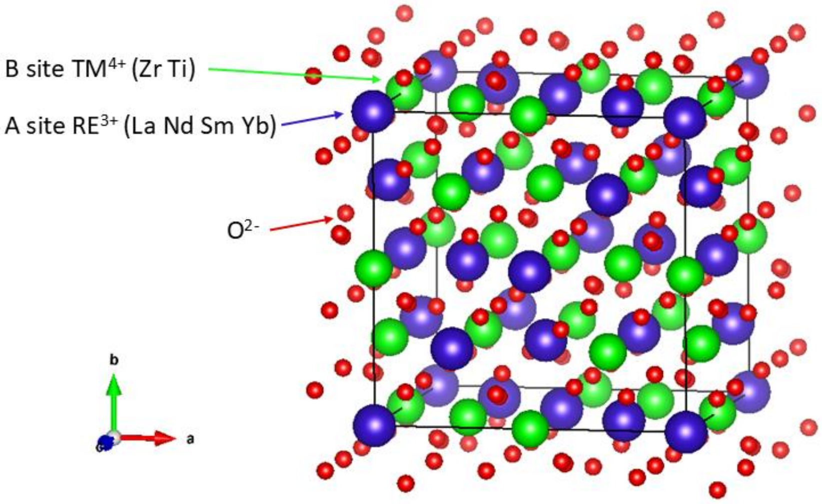

**Figure III.4**: Crystal structure of the $(Sm,Nd,La,Yb)_2(Ti_{0.5},Zr_{0.5})_2O_7$ compound visualized using VESTA software, showing the typical cubic pyrochlore structure (space group Fd-3m). Rare-earth elements occupy the A-sites, while Ti and Zr occupy the B-sites in the $BO_6$ octahedra. Oxygen atoms form a three-dimensional framework, with partial vacancies typical of pyrochlore-type oxides. The visualization highlights the atomic ordering and coordination environments within the unit cell.

## III.5. Dilatometry (DL)

The temperature dependent dilatometric behavior of sintered $(Nd_{0.25}Sm_{0.25}La_{0.25}Yb_{0.25})_2(Zr_{0.5}Ti_{0.5})_2O_7$ ceramics is depicted in (Figure III.5). The linear dimensional change demonstrates a monotonic increase with rising temperature, consistent with the thermal expansion behavior of pyrochlore-structured materials (space group $Fd\overline{3}m$) [6]. This phenomenon is primarily attributed to the amplification of atomic vibrational amplitudes at elevated temperatures, which induces a progressive expansion in the interatomic lattice spacing. As thermal energy increases, the resultant augmentation of atomic oscillation amplitudes drives volumetric expansion of the ordered pyrochlore lattice, manifesting as quantifiable linear dimensional changes. Such thermally induced dimensional variation aligns with the intrinsic thermomechanical response of $A_2B_2O_7$-type pyrochlores, where the rigid framework of corner-sharing $BO_6$ octahedra and A site cation coordination governs thermal stability [7,8]. These experimental observations corroborate the structural integrity and thermal resilience of the $(Nd_{0.25}Sm_{0.25}La_{0.25}Yb_{0.25})_2(Zr_{0.5}Ti_{0.5})_2O_7$ ceramic system at elevated temperatures, further supporting its classification as a defect-tolerant pyrochlore rather than a disordered fluorite structure [9].

The thermal expansion coefficient (CTE) of $(Nd_{0.25}Sm_{0.25}La_{0.25}Yb_{0.25})_2(Zr_{0.5}Ti_{0.5})_2O_7$ ceramics was determined to be $7.27 \times 10^{-6}\ °C^{-1}$ within the temperature range of 100–1200°C. This value is lower than that of unsubstituted $Ln_2Zr_2O_7$ pyrochlores (typically ~8–10 × $10^{-6}\ °C^{-1}$) [10], likely due to the partial substitution of $Zr^{4+}$ with $Ti^{4+}$, which introduces lattice strain and reduces atomic vibrational amplitudes [11]. Compared to conventional zirconia-based ceramics (~10 × $10^{-6}\ °C^{-1}$) [12], the studied system demonstrates enhanced thermal stability, making it suitable for high-temperature structural applications where dimensional mismatch is critical. The observed CTE aligns with the defect-tolerant pyrochlore framework of the material, where the rigid corner-sharing $BO_6$ octahedra (B = Zr/Ti) and mixed A-site occupancy (Nd/Sm/La/Yb) synergistically moderate thermal expansion [11]. This balance positions the ceramic as a promising candidate for thermal barrier coatings or refractory components in oxidizing environments up to 1200°C, outperforming silicon-based ceramics (~1600°C limit) in specific high-stress scenarios [13].

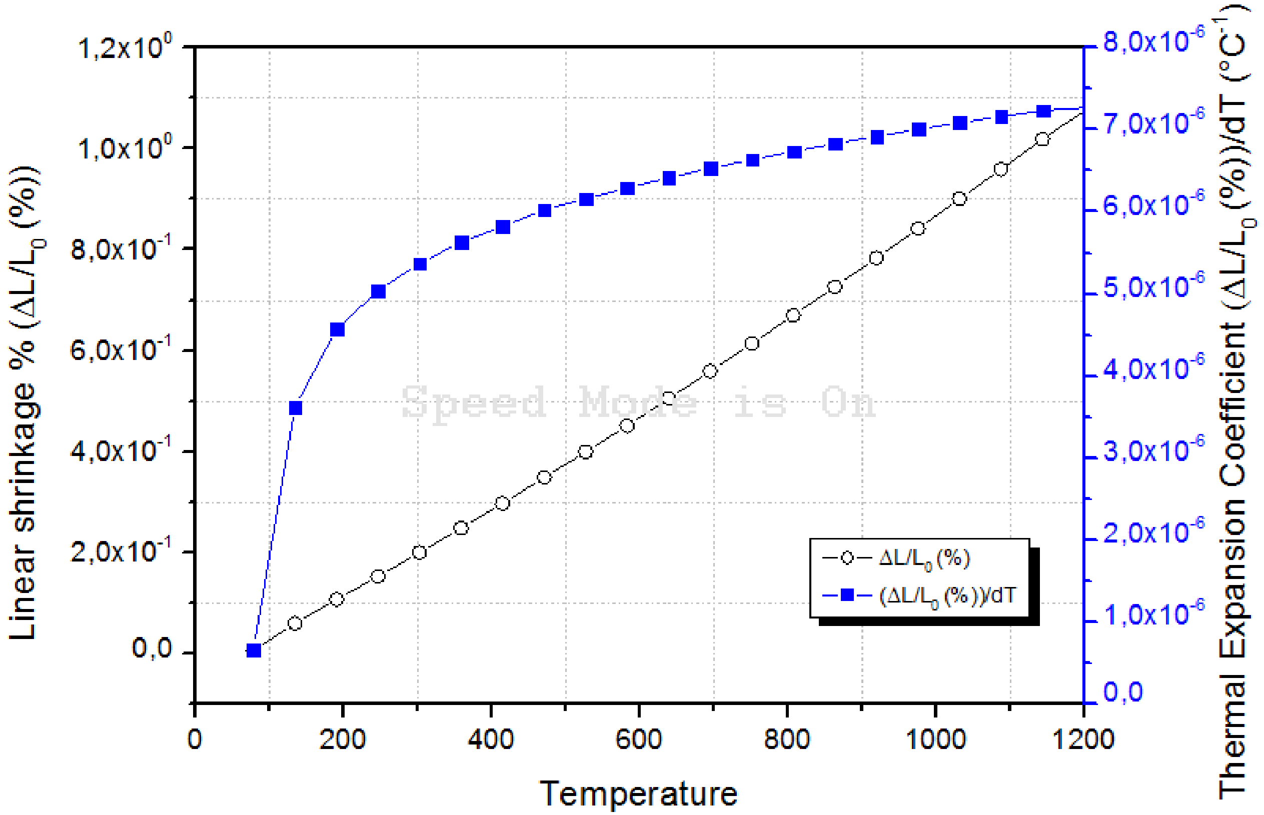

**Figure III.5**: The temperature dependence of linear shrinkage ($\Delta L/L_0\%$) and the linear thermal expansion coefficient ($\alpha$) for the $(Nd_{0.25}Sm_{0.25}La_{0.25}Yb_{0.25})_2(Zr_{0.5}Ti_{0.5})_2O_7$ sample sintered at 1500 °C for 4 hours.

## III.6. Microstructural and EDX Analysis

The microstructure, morphologies and elemental distribution of $(Nd_{0.25}Sm_{0.25}La_{0.25}Yb_{0.25})_2(Zr_{0.5}Ti_{0.5})_2O_7$ ceramic sintered at 1500 °C for 4 hours were analyzed using a Scanning Electron Microscopy (SEM) equipped with an Energy-dispersive X-ray spectroscopy (EDX) analysis.

The microstructure and elemental distribution of the sintered $(Nd_{0.25}Sm_{0.25}La_{0.25}Yb_{0.25})_2(Zr_{0.5}Ti_{0.5})_2O_7$ ceramic are critical to understanding its thermal and mechanical behavior. Here, we analyze the surface (Figure III.6a) and fractured interior microstructures (Figure III.6b) and energy-dispersive X-ray spectroscopy (EDX) (Figure III.7) results, contextualized with prior studies on pyrochlore ceramics.

### a. Microstructural Characterization

### a.1. Surface Morphology (Figure III.6a)

The surface SEM image (Figure III.6a) reveals a dense, polycrystalline microstructure typical of sintered pyrochlore ceramics. Key features include:

- **Grain Size and Shape**: Equiaxed grains with an average size of ~1–5 μm, consistent with solid-state sintering at high temperatures (likely >1400°C). The uniformity in grain size suggests controlled grain growth, minimizing abnormal grain coarsening that can degrade mechanical properties [14].

- **Porosity**: Minimal visible porosity (<5% area fraction), indicating near-theoretical density. This aligns with the material's high thermal stability, as porosity acts as a site for crack initiation under thermal stress.

### a.2. Fractured Interior Morphology (Figure III.6b)

The fractured surface (Figure III.6b) provides insight into grain boundary strength and fracture mechanisms:

- **Fracture Mode**: Predominantly transgranular fracture (cracks propagate through grains), indicating strong grain boundaries. This is characteristic of pyrochlores with high bond strength between A-site cations (Nd/Sm/La/Yb) and the $BO_6$ octahedral framework (Zr/Ti) .

- **Grain Boundary Structure**: Smooth, well-defined grain boundaries without visible secondary phases or voids, supporting the high sinterability inferred from the surface image.

### b. EDX Analysis

Energy-dispersive X-ray spectroscopy (EDX) analysis (Figure III.7) was performed on several regions of the sample surface to determine the elemental distribution. The results confirmed the presence of Sm, Nd, La, Yb, Ti, and Zr in approximately consistent proportions, indicating a relatively homogeneous distribution of these elements on the microscale. No significant elemental segregation or structural discontinuities were observed, supporting the formation of a compositionally uniform phase. This elemental homogeneity reflects the successful incorporation of multiple cations into a single matrix, a key feature of high-entropy oxides.

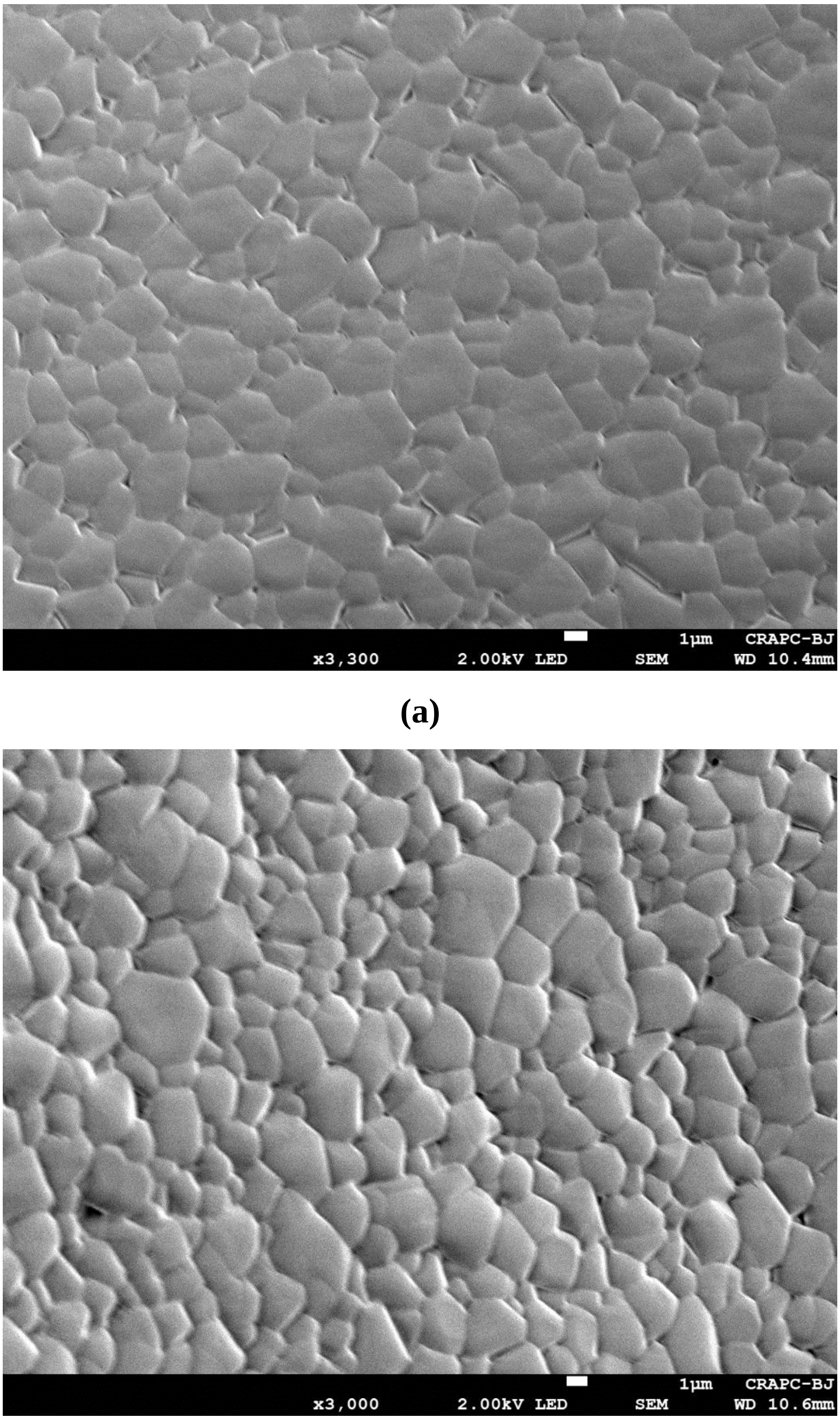

**(a)**

**(b)**

**Figure III.6**: SEM images of $(Nd_{0.25}Sm_{0.25}La_{0.25}Yb_{0.25})_2(Zr_{0.5}Ti_{0.5})_2O_7$ sample sintered at 1500°C for 4h, where (a) the surface and fractured interior (b).

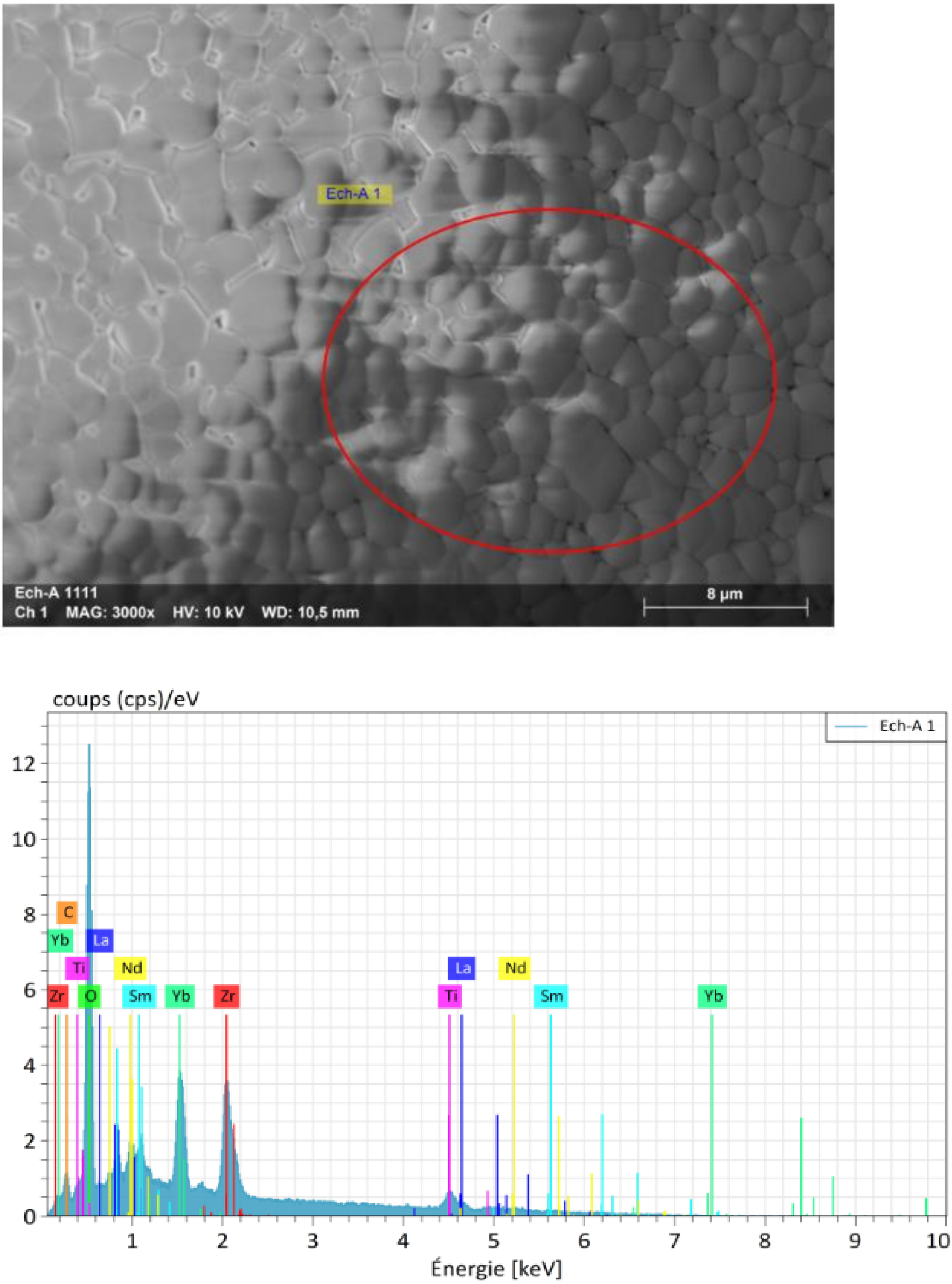

**Figure III.7**: EDX analysis of $(Nd_{0.25}Sm_{0.25}La_{0.25}Yb_{0.25})_2(Zr_{0.5}Ti_{0.5})_2O_7$ sample sintered at 1500°C for 4h.

## References

[1] R. Shannon, ‘Revised Effective Ionic Radii and Systematic Studies of Interatomic Distances in Halides and Chalcogenides’, Acta Cryst, vol. 32, pp. 751–767, Jan. 1976.

[2] W. Fan, Y. Bai, Y. Liu, T. Li, B. Li, L. Zhang, and H. Han, ‘Principal element design of pyrochlore-fluorite dual-phase medium- and high-entropy ceramics’, J. Mater. Sci. Technol., vol. 107, pp. 149–154, Apr. 2022.

[3] K. Foger, M. Hoang, T.W. Turney, ‘Formation and thermal decomposition of rare-earth carbonates’, J Mater Sci, vol. 27, pp. 77–82, 1992.

[4] R. Alvero, I. Carrizosa, J.A. Odriozola, J.M. Trillo, ‘Hydration of $Sm_2O_3$ under mild conditions’, J Less Common Met, vol. 109, no. 2, pp. 197–207, 1985.

[5] Y. T. Matulevich, M. S. Lee, J. H. Kim, J. S. Choi, S. K. Kim, S. S. Suh, M. Kirm, Ion-induced electron emission from different crystalline phases of $ZrO_2$, Applied physics letters , vol. 88, no. 21, 2006.

[6] K. Holliday, S. Finkeldei, S. Neumeier, C. Walther, D. Bosbach, T. Stumpf, ‘TRLFS of $Eu^{3+}$ and $Cm^{3+}$ doped $La_2Zr_2O_7$: A comparison of defect fluorite to pyrochlore structures’, Journal of Nuclear Materials, vol. 433, no. 1–3, pp. 479–485, Feb. 2013.

[7] A.J. Burggraaf, T. van Dijk, M.J. Verkerk, ‘Structure and conductivity of pyrochlore and fluorite type solid solutions’, Solid State Ionics, vol. 5, pp. 519–522, Oct. 1981.

[8] L. Kong, Z. Wang, I. Karatchevtseva, Y. Zhang, ‘Phase transition in $Eu_2Zr_{2-x}O_{7-2x}$ (x = 0 1) solid solutions: A combined structural and spectroscopic study’, JAmCeramSoc, vol. 107, pp. 7604–7618, 2024.

[9] I.A. Bajenova, A.V. Guskov, P.G. Gagarin, A.V. Khvan, V.N. Guskov, K.S. Gavrichev, ‘Enthalpies of formation of pyrochlore $Tb_2Hf_2O_7$ and fluorite $RE_2O_3{\cdot}2HfO_2$ (RE = Dy–Lu) rare-earth hafnates’, J Am Ceram Soc, 2025.

[10] Z. Peng, Y. Wang, S. Wang, J. Yao, Q. Zhao, E. Xie, G. Chen, Z. Wang, Z. Liu, Y. Wang, J. Ouyang, ‘Improvement strategy on thermophysical properties of $A_2B_2O_7$type rare earth zirconates for thermal barrier coatings applications: A review’, International Journal of Minerals, Metallurgy and Materials, vol. 31, no. 5, pp. 1147–1165, 2024.

[11] R. Qiu, C. Yi, X. Xiao, X. Huang, Z. Xiao, H. Dong, X. Li, L. Kong, Z. Fu, ‘Research and Application Progress of Low Thermal Expansion Ceramic Materials’, J.of Ceramics, vol. 45, no. 5, 2024.

[12] N. Juntavee, C. Dangsuwan, ‘Role of coefficient of thermal expansion on bond strength of ceramic veneered yttrium-stabilized zirconia’, J Clin Exp Dent, vol. 10, no. 3, pp. e279–e286, Mar. 1, 2018.

[13] J.F. Justin, A. Jankowiak, ‘Ultra High Temperature Ceramics: Densification, Properties and Thermal Stability’, J Aero Space Lab, no. 3, Nov. 2011.

[14] Z.G. Liu, J.H. Ouyang, Y. Zhou, X.L. Xia, ‘Effect of Ti substitution for Zr on the thermal expansion property of fluorite-type $Gd_2Zr_2O_7$’, Materials and Design, vol. 30, pp. 3784–3788, 2009.

# General Conclusion

# General Conclusion

This study presents a comprehensive analysis of the composition and properties of high-entropy pyrochlore ceramics $(Nd_{0.25}Sm_{0.25}La_{0.25}Yb_{0.25})_2(Zr_{0.5}Ti_{0.5})_2O_7$, with a focus on its relationship to high-temperature applications. Through the combination of various analytical techniques (TG/DTG, DTA, XRD, SEM/EDX), it was confirmed that the system exhibits an ordered pyrochlore structure under appropriate sintering conditions, where the ionic radius ratio ($r(A)/r(B) \approx 1.64$) confirmed phase stability within the theoretical range (1.46–1.78).

The results of thermal analysis (TG/DTA) showed that mass loss occurs in multiple stages associated with the decomposition of precursors (hydroxides and carbonates of rare earth elements) up to 850°C, followed by stabilization of the sample mass at higher temperatures, indicating the formation of a single crystalline pyrochlore phase. XRD results also confirmed that sintering at 1400°C leads to the formation of an ideal pyrochlore structure (matching the PDF#00-024-1012 reference), with the absence of secondary phases.

In terms of thermal properties, the coefficient of thermal expansion (CTE) recorded a relatively low value ($7.27 \times 10^{-6}$ °C$^{-1}$) compared to unsubstituted pyrochlore ceramics, which enhances its suitability for applications requiring dimensional stability under thermal stress, such as Thermal Barrier Coatings (TBCs). SEM images also showed a dense microstructure with homogeneous element distribution, supporting the material's durability and suitability for use in oxidizing environments up to 1200°C.

This study provides a qualitative addition to the field of energy and environmental materials, showing the potential of using high-entropy pyrochlores as alternative materials to traditional ceramics (such as zirconia or silicon-based) in high-temperature requirement applications. It also opens the door for further research into the effect of ion substitution on radiation tolerance and ionic conductivity properties, which may expand their application range in the field of nuclear energy or catalysis.

On the recommendations side, future studies are advised on:

1. The effect of different substitution ratios of rare earth elements on phase stability.

2. Evaluation of mechanical properties (toughness, hardness) under cyclic stress conditions.

3. Study the Optical and Electrical properties.

In summary, the results of this study show that $(\mathrm{Nd}_{0.25}\mathrm{Sm}_{0.25}\mathrm{La}_{0.25}\mathrm{Yb}_{0.25})_2(\mathrm{Zr}_{0.5}\mathrm{Ti}_{0.5})_2\mathrm{O}_7$ represents a promising candidate for the development of advanced ceramic materials that meet the requirements of modern engineering applications in the field of energy and space.

# ABSTRACT

The pyrochlore structure has the general formula $A_2B_2O_7$, where the A-site is typically occupied by trivalent rare-earth elements, and the B-site contains tetravalent transition metal elements. Owing to the wide range of both elements A and B sites, a larger number of pyrochlore ceramics have been developed through introducing partial substitutes or doping into A and B sites. In this study, the $A_2B_2O_7$ (A = La, Sm, Nd, Yb; B= Zr, Ti) ceramics with a pyrochlore phase structure were sucessfully synthesized using a high temperature solid-state reaction method and its characterization, morphology, structural and thermal properties were summarized. The **$A_2B_2O_7$** samples calcinated at various temperatures were investigated by using a series of technique, such as Thermogravimetry (TG), Differential Thermal Analysis (DTA), X-ray diffraction (XRD), Dilatometry (DIL), Scanning Electron Microscopy (SEM), and Energy-dispersive X-ray spectroscopy (EDS) , in order to follow and characterize the crystalline phases and their transformation as a function of temperature. The results show that the prepared samples have a single-phase of pyrochlore structure, and all presented elements are distributed homogeneously at A and B sites, respectively. The material exhibits a thermal expansion coefficient (CTE) of $7.27 \times 10^{-6}$ °$C^{-1}$ over the temperature range of 100 to 1200 °C. The results conclude by discussing how high-entropy oxide ceramics will be used in various future applications.

**Key Words:** Pyrochlore, rare-earth elements, solid-state reaction, high-entropy oxide ceramics

# RÉSUMÉ

La structure pyrochlore a la formule générale $A_2B_2O_7$, où le site A est typiquement occupé par des éléments de terres rares trivalents, et le site B contient des éléments métalliques de transition tétravalents. En raison de la large gamme des éléments sur les sites A et B, un plus grand nombre de céramiques pyrochlores ont été développées en introduisant des substituts partiels ou un dopage dans les sites A et B. Dans cette étude, les céramiques $A_2B_2O_7$ (A = La, Sm, Nd, Yb ; B = Zr, Ti) avec une structure de phase pyrochlore ont été synthétisées avec succès en utilisant une méthode de réaction à l'état solide à haute température, et leur caractérisation, morphologie, propriétés structurales et thermiques ont été résumées. Les échantillons $A_2B_2O_7$ calcinés à différentes températures ont été étudiés en utilisant une série de techniques, telles que la thermogravimétrie (TG), l'analyse thermique différentielle (ATD), la diffraction des rayons X (DRX), la dilatométrie (DIL), la microscopie électronique à balayage (MEB) et la spectroscopie à dispersion d'énergie (EDS), afin de suivre et de caractériser les phases cristallines et leur transformation en fonction de la température. Les résultats montrent que les échantillons préparés possèdent une phase unique de structure pyrochlore, et tous les éléments présentés sont respectivement distribués de manière homogène sur les sites A et B. Le matériau présente un coefficient de dilation thermique (CDT) de $7,27 \times 10^{-6}$ °$C^{-1}$ sur la plage de températures de 100 à 1200 °C. Les résultats concluent en discutant de la manière dont les céramiques d'oxyde à haute entropie seront utilisées dans diverses applications futures.

**Mots clés :** Pyrochlore, éléments de terres rares, réaction à l'état solide, céramiques d'oxyde à haute entropie

# الملخص

يحتوي هيكل البيروكلور (pyrochlore) على الصيغة العامة$A_2B_2O_7$ ، حيث عادةً ما يشغل الموقع A عناصر الأرض النادرة ثلاثية التكافؤ، ويحتوي الموقع B على عناصر معدنية انتقالية رباعية التكافؤ. نظرًا لتنوع العناصر في مواقع A وB ، فقد تم تطوير عدد أكبر من سيراميك البيروكلور من خلال إدخال بدائل جزئية أو تشويب في مواقع A و .B في هذه الدراسة، تم تصنيع عينات $A_2B_2O_7$ (A = La, Sm, Nd, Yb; B= Zr, Ti)ذات بنية طور البيروكلور بنجاح باستخدام طريقة تفاعل الحالة الصلبة ذات درجة الحرارة العالية وتم تلخيص خصائصها، والتشكيل، والخصائص الهيكلية والحرارية. تم فحص عينات $A_2B_2O_7$ الملبدة عند درجات حرارة مختلفة باستخدام سلسلة من التقنيات، مثل قياس االتحليل الحراري الوزني (TG) ، والتحليل الحراري التفاضلي (DTA)، وحيود الأشعة السينية(XRD) ، والقياس التمدد الطولي (DIL) ، والمجهر الإلكتروني الماسح(SEM) ، والتحليل الطيفي بالأشعة السينية الموزعة للطاقة(EDS) ، من أجل متابعة وتوصيف الأطوار البلورية وتحولاتها كدالة لدرجة الحرارة. تظهر النتائج أن العينات المحضرة لها طور واحد من هيكل البيروكلور، وأن جميع العناصر المقدمة موزعة بشكل متجانس في مواقع A و B على التوالي. يعرض المادة معامل تمدد حراري (CTE) قدره $7,27 \times 10^{-6}$ °$C^{-1}$في نطاق درجة الحرارة من 100 إلى 1200 درجة مئوية. تختتم النتائج بمناقشة كيفية استخدام سيراميك أكسيد عالية المحتوى الحراري في تطبيقات مستقبلية متنوعة.

**الكلمات المفتاحية:** البيروكلور، عناصر الأرض النادرة، تفاعل الحالة الصلبة، سيراميك أكسيد عالية الانتروبيا